UNIVERSITÀ DEGLI STUDI DI PADOVA

DIPARTIMENTO DI BIOLOGIA

Corso di Laurea magistrale in Molecular Biology

TESI DI LAUREA

Implications of RASAL3 gene mutations in autoimmune diseases

Relatore: Prof.ssa Chiara Rampazzo
Dipartimento di Biology

Correlatore: Dr. Aude Magérus
Immunogenetics in pediatric autoimmune diseases, Institut Imagine

Laureanda: Simona Iezzi

ANNO ACCADEMICO 2024/2025

Abstract

Autoimmune diseases result from the breakdown of self-tolerance, often due to mutations affecting key immune regulatory genes. The dysregulation of Ras-MAPK is a hallmark of several autoimmune disorders as it is implicated in crucial T and B lymphocyte functions such as proliferation, differentiation, motility, apoptosis and senescence.

Mutations of interest in the *RASAL3* gene were identified in five patients suffering from either pediatric auto-immune hepatitis (AIH) or Evans syndrome using whole exome sequencing and subsequently confirmed by Sanger sequencing and segregation analysis.

RASAL3 encodes a RasGAP protein that negatively regulates the Ras-MAPK pathway, which is essential in BCR/TCR-mediated lymphocyte homeostasis and activation. Given its role in modulating T cell responses, alterations in RASAL3 could lead to aberrant immune activation and autoimmunity.

To investigate this hypothesis, a cellular model was established using Jurkat T cells and B-LCLs to monitor pERK induction following TCR- and BCR-mediated activation of the Ras pathway. Additionally, HEK cells were employed to explore the signaling context of RASAL3 through the generation of expression plasmids harboring mutant RASAL3 sequences and the optimization of Ras pathway stimulation conditions.

Table of Contents

INTRODUCTION

1. *The immune system*

The immune system is a highly complex and dynamic network composed of cellular elements, soluble proteins, and chemical mediators that protect the body from foreign substances, including pathogens and tumor cells, while maintaining tolerance to self-antigens. The ability to distinguish self from non-self relies on specific recognition molecules expressed on the membranes of immunocompetent cells.

The regulation of this intricate system involves a vast array of soluble mediators and intracellular signaling events, such as phosphorylation cascades. Ultimately, the integration of membrane receptor engagement with intracellular signaling determines the functional outcomes of immune cells, including apoptosis, maturation, proliferation, and survival, which are essential processes for a coordinated and effective immune response.
Immune tolerance is a crucial mechanism for the maintenance of homeostasis and health. The immune properties of B and T cells, such as their ability to interact with other immune cells and cytokines around them, allow them to build a complex network of immune tolerance. The principal goal for this network is to avoid autoreactive lymphocytes that lead to uncontrolled immune response.

Immunity can be broadly divided into innate and adaptive branches. While innate immunity provides immediate, germline-encoded recognition and response, adaptive immunity is characterized by specific-antigen receptors and the generation of immunological memory. The central effectors of adaptive immunity are T and B lymphocytes, which express T cell receptors (TCRs) and B cell receptors (BCRs) generated via gene recombination and a rigorous selection process.

Upon antigen recognition, these receptors initiate complex intracellular signaling cascades, including those involving the RAS–MAPK pathway, that drive cell activation, proliferation, and effector functions, ensuring a tailored and efficient immune response. (Bonnerot et al., 1997; Chaplin, 2010)

1. *T cells and TCR*

T cells play a central role in maintaining immune tolerance. They develop and mature in the thymus under the influence of thymic hormones and peptides. T cell recognizes antigens only after they have been processed into peptide fragments and presented on the cell surface by major histocompatibility complex (MHC) molecules. The antigen recognition molecule of T lymphocytes is the T-cell receptor (TCR), a heterodimeric transmembrane protein. The interaction between the TCR, the antigenic peptide, and the MHC molecule is highly specific and tightly regulated.

The TCR complex consists of two TCR chains and six clusters of differentiation 3 (CD3) chains, which are essential to mediate intracellular signals.

Full T-cell activation requires not only TCR engagement but also co-receptors and additional signaling pathways initiated by other surface molecules. The mechanism of initiation of TCR signaling remains enigmatic several models have been proposed, about the sensitivity for specific affinity threshold: below this value, the response does not occur. (Courtney et al., 2018)
The mechanical reception of cognate antigen by the extracellular TCR and subsequent intracellular changes in the CD3 complex is a prerequisite for T cell activation and the generation of T cell-mediated adaptive immunity. (Shah et al., 2021)

Upon engagement with the corresponding peptide-MHC complex (pMHC), the intracellular TCR signaling is initiated via the immunoreceptor tyrosine-based motif (ITAMs) in the cytoplasmic domains of CD3 proteins. When this motif is phosphorylated it can bind the Src Homology 2 (SH2) domain of several proteins, specifically ZAP-70, which undergoes conformational activation and propagates downstream signals. One key downstream target is the linker of activation of T cells (LAT), whose phosphorylation triggers several signaling cascades, like phospholipase C gamma 2 (PLCγ2) that activates the Ca2+ signaling and RAS/MAPK pathway, the recruitment of Grb2 and Gads, adaptors that bind SOS and SLP-76 which can lead to Ras, Rac, Rho GTPase activation, among other effector responses. (Kortum et al., 2013)

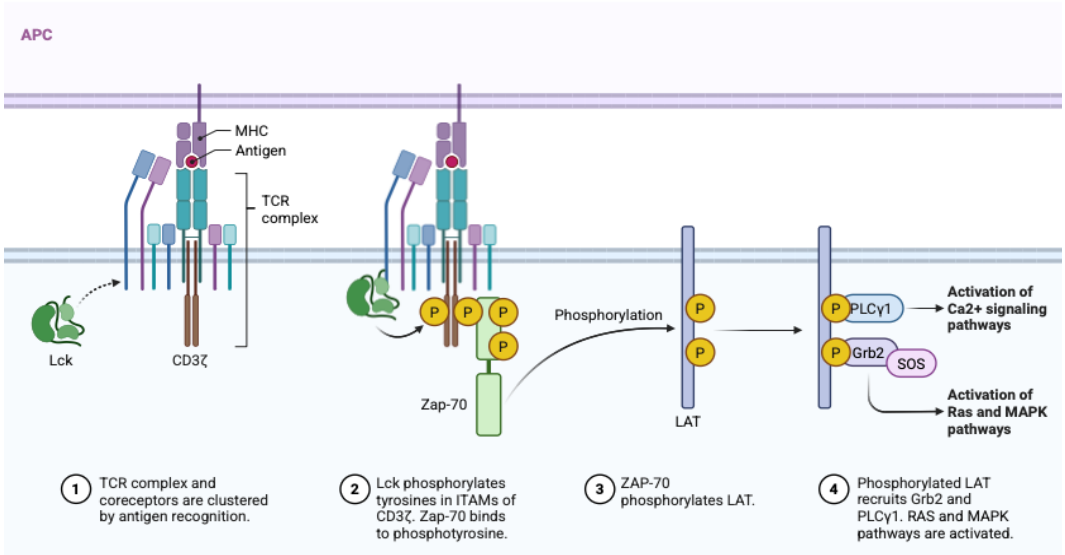

Figure 1: Overview of the major TCR-activation signaling pathways.
Antigen recognition by the TCR complex and co-receptors leads to their clustering on the T cell surface (1). The Src-family kinase Lck phosphorylates tyrosine residues within the ITAM motifs of CD3ζ, enabling the recruitment and activation of the kinase ZAP-70 (2). Activated ZAP-70 subsequently phosphorylates the adaptor protein LAT (3). Activation of LAT-associated effector molecules results in signal propagation via three major signaling pathways: the Ca2+–calcineurin, mitogen-activated protein kinase (MAPK), nuclear factor-κB (NF-κB) signaling pathways. (BioRender)

2. *B cells and BCR*

As T cells also B cells are equipped with a unique surface molecule known as the B Cell Receptor (BCR), which allows them to recognize and respond to specific antigens (Cyster & Allen, 2019).

The BCR is composed of a pair of heavy- and light-chain immunoglobulins which are the result of random rearrangement of immunoglobulin genes, creating a unique antigen-binding site.
As the membrane-bound immunoglobulin has a cytoplasmic tail that is very short, it is not in itself signaling-competent, but it is associated with the CD79A and CD79B subunits, each of which carries one immunoreceptor tyrosine-based activation motif (ITAM) in their intracellular domains.

Once BCR interacts with a specific antigen, based on the intensity of the stimuli, it could induce the intracellular signaling that is essential for B cell development and maturation. A unified molecular mechanism explaining how the target antibody triggers BCR activation has yet to be defined (Degn & Tolar, 2025).

Upon antigen engagement, the B cell receptor (BCR) initiates a signaling cascade through its associated transmembrane proteins, CD79A and CD79B, which each contain ITAMs. These ITAMs harbor two conserved tyrosine residues that are rapidly phosphorylated by members of the SRC-family kinases, particularly LYN, FYN, and BLK, which are predominant in B cells. The dual phosphorylation of ITAMs creates high-affinity docking sites for the Spleen Tyrosine Kinase (SYK) via its tandem Src homology 2 (SH2) domains, thereby initiating downstream signaling.

Notably, CD79A possesses an additional tyrosine residue outside of the ITAM that is also phosphorylated by SRC-family kinases. This site facilitates the recruitment of the adaptor protein BLNK. Upon recruitment, SYK becomes activated and subsequently phosphorylates BLNK, promoting the assembly of a multi-protein signaling complex.
The formation of signalosome drives the activation of multiple pathways, including calcium flux, protein kinase C (PKC) activation, and MAPK signaling, ultimately leading to changes in gene expression required for B cell activation, proliferation, and differentiation, through the mediation of extracellular signal-regulated kinase (ERK) phosphorylation.
These events may additionally be supported by signaling via CD19, which is part of the BCR co-receptor complex. Phosphorylation of CD19 by SRC kinases enhances the recruitment of phosphatidylinositol-3 kinases (PI3Ks), which produce phosphatidylinositol (3,4,5)-trisphosphate (PIP3). Accumulation of PIP3 in the membrane leads to activation of AKT kinases and several downstream effects, such as the activation of the mTOR complex. (Wen et al., 2019)

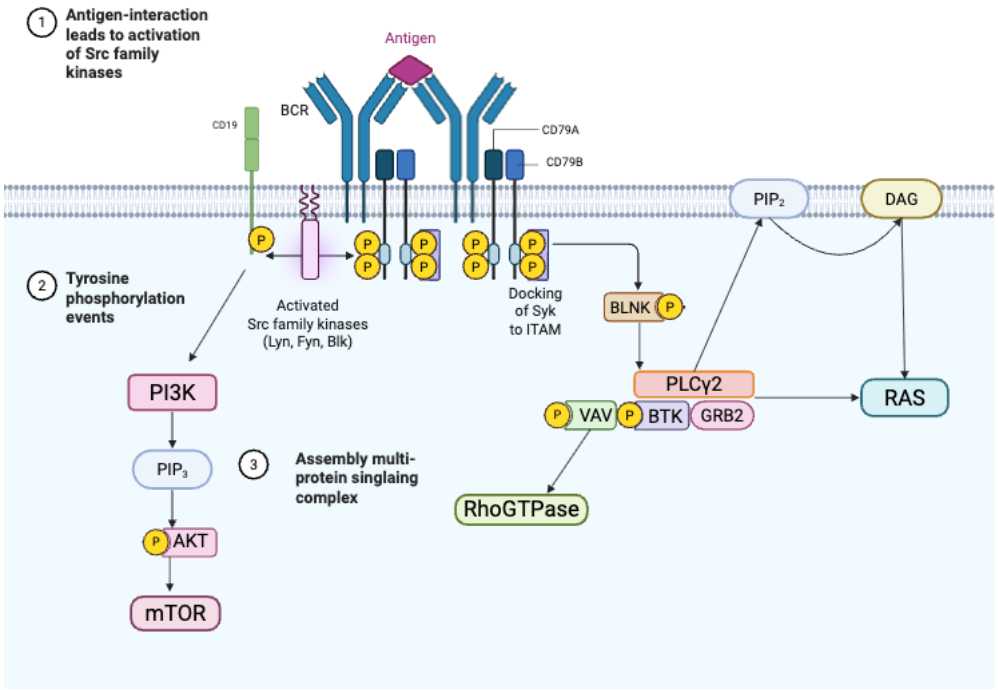

Figure 2: Intracellular signaling cascade downstream of B cell receptor (BCR) activation.
Upon antigen binding, the BCR complex undergoes conformational changes that lead to the activation of Src family kinases (e.g., Lyn, Fyn, Blk), which phosphorylate ITAM motifs on CD79A and CD79B (1–2). These phosphorylation events enable the recruitment of Syk kinase and initiate the assembly of a multi-protein signaling complex (3). Key downstream pathways include PI3K/AKT/mTOR signaling, Rho GTPase activation via VAV, and PLCγ2-mediated hydrolysis of PIP_2 to generate DAG, contributing to RAS activation. These pathways collectively regulate B cell proliferation, survival, and differentiation. (made with Biorender)

Once activated, beyond their role as antibody producers, B cells also function as potent antigen-presenting cells (APCs) that are critical for the activation and regulation of T cells, particularly $CD4^+$ helper T cells.

3. *RAS pathway*

The activation of RAS is correlated with a kinase cascade that culminates with the phosphorylation of mitogen-activated protein kinase (MAPK). MAPK pathways relay, amplify and integrate signals from a diverse range of stimuli and elicit an appropriate physiological response including cellular proliferation, differentiation, development, inflammatory responses and apoptosis in mammalian cells. (Zhang and Liu, 2002). The MAPK pathway is also known to be involved in regulating immune responses through its roles in cell proliferation, differentiation, and survival.

The final target of this pathway is ERK, which is activated by MEK-mediated phosphorylation. Notably, ERKs phosphorylate and activate a series of transcription factors such as Elk, c-Fos, p53, Ets1/2, and c-Jun, which are important for the initiation and regulation of proliferation. Alternatively, the ERKs can transmit the signal further by phosphorylating and activating protein kinases at the

MAPK pathway. One of the targets of ERK is the ribosomal S6 kinases (RSKs), which can independently translocate into the nucleus and phosphorylate a distinct set of substrates there (Liu et al., 2007).

Another target of RAS is the PI3k pathway that culminates with the activation of AKT and the consequent mTOR pathway (Powell et al., 2012). It leads to increased lipid production, ribosome biosynthesis, mRNA synthesis, and protein translation. One of the targets of mTORC is p70 ribosomal S6 kinase (p70-RS6K), which is involved in regulating protein synthesis, cell size, cell-cycle progression, glucose homeostasis by phosphorylating S6 Ribosomal Protein (S6RP), a component of eukaryotic ribosomes. Accumulating evidence suggests that also p90 ribosomal S6 kinase (p90-RS6K) can play a role in S6RP phosphorylation on Ser235/236 through an mTOR-independent mechanism.

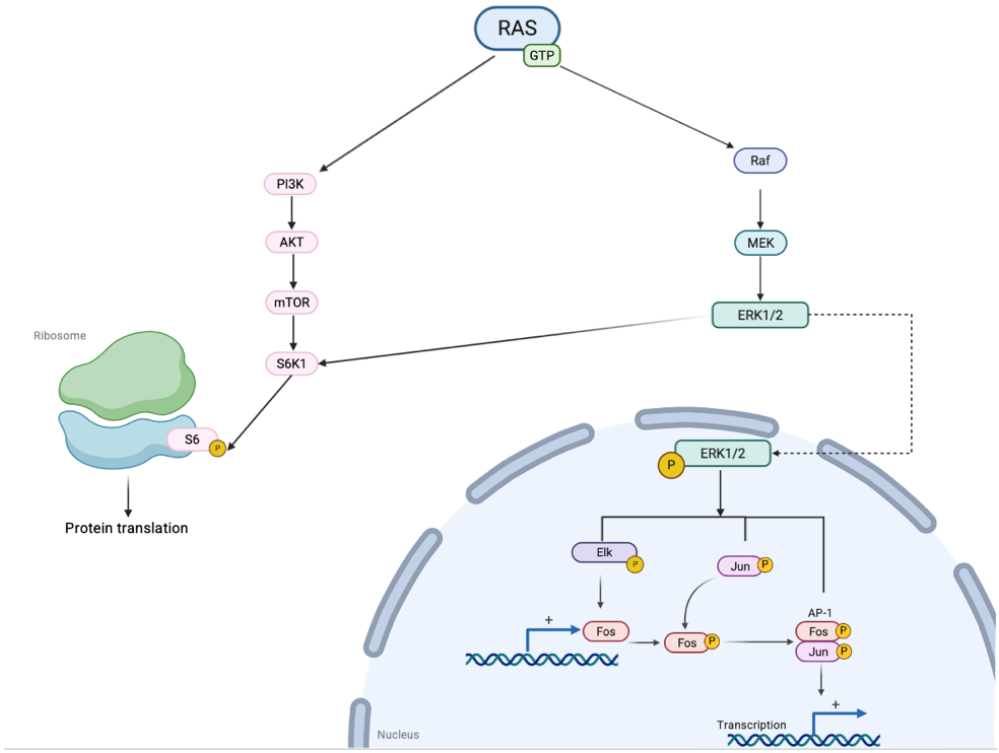

Figure 3: RAS-mediated activation of MAPK/ERK and PI3K/AKT/mTOR signaling pathways.
Upon activation, GTP-bound RAS triggers two major signaling cascades. The first leads to the activation of the PI3K–AKT–mTOR pathway, culminating in the phosphorylation of ribosomal protein S6 via S6K1, thereby promoting protein translation. The second involves the canonical MAPK pathway, in which RAS activates Raf, initiating the MEK–ERK1/2 cascade. Phosphorylated ERK1/2 translocates to the nucleus, where it activates transcription factors such as Elk and Jun. This results in the upregulation of immediate early genes, including Fos, and the formation of the AP-1 transcriptional complex (Fos/Jun), ultimately promoting the transcription of target genes involved in proliferation and differentiation. (Biorender)

The RAS pathway is involved in many contrary effects that are induced by the same initial activated receptor (TCR or BCR). It still be unclear how the same receptor and the same intracellular pathway can lead to different cellular responses, based on the stimulus received. One possible explanation is based on the strength of the interaction between the antigen and the receptor. Other theories are based on the contribution of other coreceptors or the length of the interaction and the consequent length of the activation of the RAS pathway. The investigation of the activity of Ras inhibitor will clarify the possible way of working of this complex and highly controlled mechanism. Recently, two models of RAS activation during T-cell development have been proposed to explain how the same pathway can lead to different cellular outcomes. (Kortum et al., 2013).

4. *Autoimmune diseases*

Dysregulation of these signaling mechanisms can result in the breakdown of immune tolerance and the onset of autoimmune diseases. Autoimmune disorders encompass a wide spectrum, ranging from organ-specific conditions (in which antibodies and T cells react to self-antigens localized in specific tissues) to systemic diseases (characterized by reactivity against antigens present in multiple tissues). The incidence of autoimmune illness among identical twins ranges from 12% to 67% (Yasmeen F, 2024), highlighting the contribution of genetic, epigenetic combined with environmental factors.
Autoimmune diseases are both widespread and heterogeneous. While their pathogenesis is multifactorial, shaped by a combination of environmental influences and polygenic predispositions, a subset of monogenic autoimmune disorders has also been described, primarily in pediatric populations and often in association with primary immunodeficiencies. Notable examples include autoimmune lymphoproliferative syndrome (ALPS), linked to defects in the FAS-mediated apoptotic pathway. The study of these monogenic disorders has significantly advanced our understanding of immune tolerance mechanisms in humans, shedding light on processes such as central tolerance, receptor editing, regulatory T cell development and function, peripheral deletion of autoreactive lymphocytes and gene regulatory elements involved in antigen-specific immune responses. In addition, understanding the genetic basis of autoimmunity is essential for the development of targeted therapies.

For several autoimmune diseases, key genes have been identified whose mutations are directly associated with disease onset. However, there are instances in which individuals carrying known pathogenic haplotypes do not develop clinical phenotypes (Lucas & Lenardo, 2015).
In addition, for many autoimmune diseases, the genetic component remains indeterminate. Therefore, identifying other contributors to immune dysregulation is crucial for uncovering new disease-related genes and pathogenic mutations. Once functionally validated, genetic defects can be incorporated into diagnostic workflows for early disease diagnosis and used to develop precise, targeted therapeutic strategies or better adapt existing ones.

The research team led by Dr. Frédéric Rieux-Laucat at the Imagine Institute focuses on the immunogenetics of pediatric autoimmune diseases, particularly on mechanisms of self-tolerance failure in primary immunodeficiencies and

hyperimmune syndromes. Current efforts aim to identify genetic events that influence physiological immune processes, as these are implicated in diseases such as autoimmune hepatitis (AIH), ALPS, and Evans syndrome (ES).

Whole Exome Sequencing (WES) analysis of patients presenting with pediatric auto-immune disease revealed 5 variants with high deleterious and pathogenic scores affected the same gene: RASAL3. Notably, two patients were diagnosed with Evans Syndrome and three patients with Autoimmune Hepatitis.

Autoimmune hepatitis (AIH) is a chronic immune-mediated liver disease, characterized by circulating autoantibodies, elevated serum IgG levels, and histologic interface hepatitis. The worldwide incidence and prevalence of AIH are 1.37 and 17.44 cases/100,000, respectively (Lv et al., 2019). The incidence is lower in children: 0.35 (95% CI, 0.24–0.52) cases per 100,000 inhabitant-years (Hahn et al., 2023).

The main histological hallmark of AIH is a dense infiltrate of lymphocytes, macrophages and plasma cells in the liver and it is due to the presentation of self-antigen peptides to the TCR of uncommitted T cells and consequent hyperactivation of B cells. The symptoms are heterogeneous and vary with age, sex, subtype of disease; the diagnosis is based on the combination of clinical signs, laboratory findings, histological analysis including levels of serum transaminases, IgG levels, liver biopsy and detection of autoantibodies. AIH is recognized as a multifactorial pathogenesis in which a unique cause is usually difficult to find, but some genetic variants could contribute to the development of the disease and are currently under investigation (Nastasio et al., 2024; Terziroli Beretta-Piccoli et al., 2022).

Evans syndrome (ES) is a rare autoimmune disorder characterized by the co-occurrence of autoimmune hemolytic anemia and immune thrombocytopenia, and occasionally autoimmune neutropenia. It reflects a broader dysregulation of the immune system and can occur either as a primary condition or secondary to inborn errors of immunity.
In addition, ES may be associated with a variety of immune-mediated manifestations, including lymphoproliferation, that could lead to organ-specific inflammation, and hypergammaglobulinemia (Aladjidi et al., 2023).
Recent genomic studies have revealed that at least 65% of cases of pediatric ES may be genetically determined (Hadjadj et al., 2019).

5. <u>RASAL3</u>

RAS proteins are members of a large superfamily of low molecular-weight GTP-binding proteins, which can be divided into different families, each involved in different cellular responses. The main common characteristic is the way of function: the activation state depends on whether they are bound to GTP or GDP. Because of the low levels of intrinsic GTPase activity of RAS, there are several regulators that exchange the nucleotide: guanine nucleotide exchange factors (GEFs) and the nucleotide hydrolysis by GTPase activating proteins (GAPs). (Downward, 2002)

In this context, recent evidence has highlighted the role of RASAL3 especially involved in T-cell responses and the pathogenesis of autoimmunity.

RASAL3 acts as a GTPase-activating protein predominantly expressed in T-lineage cells and contributes to the inactivation of RAS by promoting GTP hydrolysis (Downward, 2002).
RASAL3 (Ensembl reference of transcript sequence: ENST00000343625.12) is located on chromosome 19 (19p13.12) and it is organized in 18 exons. The corresponding protein is made of 1011 aminoacids[1].

It belongs to GAP family, the members of which are characterized by a pleckstrin homology (PH), C2, and RasGAP domains (Fig.4). In particular, the RasGAP domain (a.a.458-650) is responsible for the conversion of Ras-GTP into the inactive form, Ras-GDP (Fig.4). In addition, Ca2+-dependent phospholipid-binding/conserved region 2 (C2) is necessary for dynamic membrane association following intracellular calcium release. The protein also contains lipid-binding domains that may be involved in the localization and targeting of their respective protein hosts, mediating stimulus-dependent membrane association. (Scheffzek & Shivalingaiah, 2019)

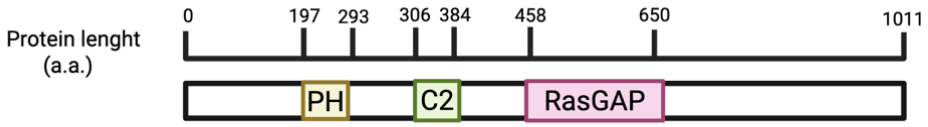

Figure 4: Schematic representation of the domain architecture of RASAL3 (1011 amino acids).
The protein contains a pleckstrin homology (PH) domain (aa 197–293), a C2 domain (aa 306–384), and a Ras GTPase-activating protein (RasGAP) domain (aa 458–650) (made with Biorender).

The expression of *RASAL3* has been detected in several hematopoietic tissues and in particular in T cell subpopulations (Fig.5).

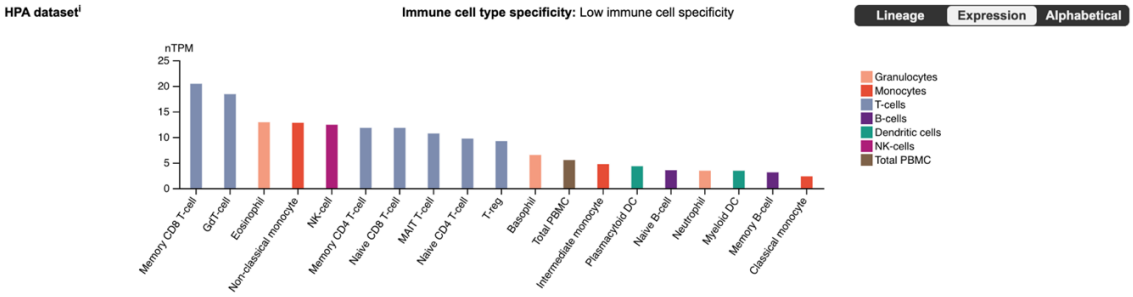

Figure 5: RASAL3 RNA expression from The Human Protein Atlas (https://www.proteinatlas.org/ENSG00000105122-RASAL3)

[1] National Center for Biotechnology Information (NCBI) from https://www.ncbi.nlm.nih.gov/protein/NP_001334956.1

By inducing overexpression of *RASAL3* cDNA in double positive Thymoma cell line (DPK)[2] the TCR-induced activation of RAS is impaired, confirming the functional role of RASAL3 as RasGAP activator (Fig.6A).

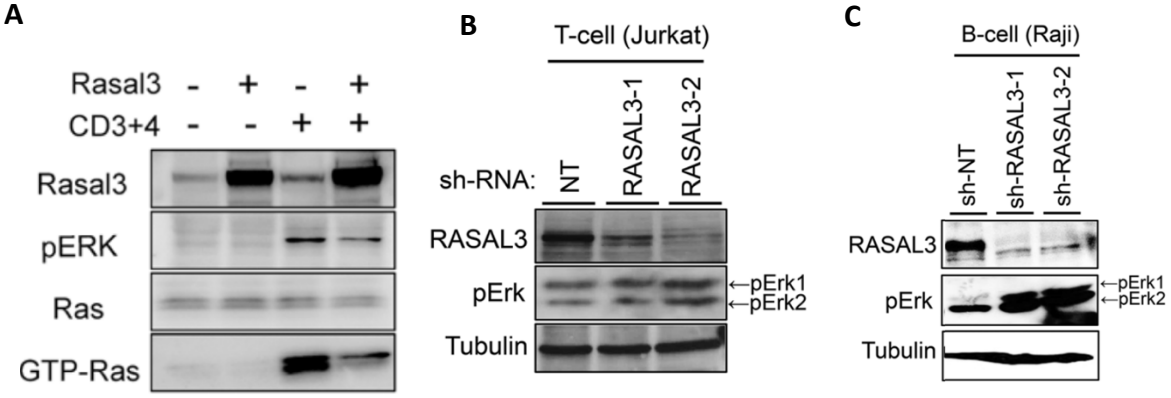

Figure 6: RasGAP activity of Rasal3:
(A) DPK cells overexpressing Rasal3 were subjected to a Ras-GTP pull-down assay followed by Western blot analysis (Muro et al., 2015). The RASAL3 expression in the human T-cell line (Jurkat)(B) and B cell line (Raji)(C) was characterized by a Western blot analysis with an anti-RASAL3 or anti-Tubulin antibody: the cells were infected with a lentivirus encoding RASAL3 shRNA (sh-RASAL3-1, sh-RASAL3-2) or control nontargeted shRNA (NT). (Saito et al., 2015)

Several studies on *RASAL3*-deficient mice have shown that the number of CD4 and CD8 naïve T cells only in the periphery is reduced due to the event of apoptosis and that their survival in vivo is impaired (Muro et al., 2015). In addition, the knock-out form of *RASAL3* in B cell and T cell lines increases the level of phosphorylation of ERK (Fig.6B-6C) (Saito et al., 2015).
It has been demonstrated that Rasal3 is essential also for the survival of CD4+ T cells and in vitro *RASAL3* deficient NKT cells showed augmented phosphorylation of ERK (pERK) and reduced production of IL-4 and IFN-γ (Muro et al., 2018).

Based on the following evidence, RASAL3 seems to be involved in the survival of peripheral T cells. As a negative regulator of the Ras pathway, the knockdown could be correlated with increased apoptosis, as a consequence of uncontrolled RAS downstream signaling.

Jurkat cells, a human T-cell leukemia line, are widely used to study TCR signaling due to their robust expression of TCR/CD3 complexes and downstream signaling molecules (Abraham & Weiss, 2004). They exhibit active Ras signaling upon stimulation, including increased GTP-bound Ras levels linked to CD3 engagement, as mediated by RasGRP and downstream of TCR signaling. This makes them an ideal model for dissecting the role of RasGAP proteins such as RASAL3 in T cell activation.
BCR activation is investigated through immortalized B lymphocytes stimulated with anti-IgM antibody.

[2] The DPK cell line is an established murine T-cell line widely used as a model for studying thymocyte development. They both CD4 and CD8 (DP phenotype) expresses functional TCR/CD3 complex, and they are capable of differentiating into $CD4^+$ single-positive cells upon antigen stimulation (Kaye J., et al. 1992).

Aims and objectives

Given RASAL3's role in modulating Ras-dependent TCR signaling and maintaining T cell survival and homeostasis, as well as its impact on pERK levels in B cells, we hypothesize that loss-of-function mutations in *RASAL3* may decrease the threshold of T cells or survival response. Such dysregulation could promote the escape and persistence of autoreactive T cell clones, contributing to the development of autoimmune diseases like AIH and ES. However, considering the complex and context-dependent role of the RAS signaling pathway, it is also conceivable that gain-of-function mutations in RASAL3 might paradoxically enhance RAS activation. Such a scenario could lead to excessive immune cell activation upon TCR/BCR engagement, promoting an aberrant immune response against self-antigens—a hallmark of the autoimmune disorders under investigation. Consequently, this research project aims to explore the molecular consequences of *RASAL3* variants, that have been identified by WES in patients presenting with Autoimmune diseases, on the TCR/RAS pathway and its downstream targets in the in vitro cell models in order to define the biological role of RASAL3 in physiological condition.
Once defining the effect of RASAL3 in the signaling pathway of T cells and B cells, it could be elucidated the role of the RAS pathway and its high regulation in the different cellular responses that immune cells can face, based on the ligand that interacts with the same receptor.

The M2 internship is focused on establishing and optimizing the experimental conditions required to functionally investigate RASAL3 mutations in vitro. The goal of this stage is to validate the cellular model and ensure it is suitable for future studies assessing the molecular consequences of RASAL3 variants.

MATERIALS AND METHODS

CELL MODELS

a) *HEK cells*

HEK 293 cells, derived from human embryonic kidney cells, exhibit epithelial morphology and adherent growth properties.
Cells were cultured DMEM (Dulbecco's Modified Eagle Medium (DMEM), Thermo Fisher Scientific, France), supplemented with 10% Fetal Bovine Serum (FBS) (Dutscher, France), 1% Penicillin-streptomycin (Thermo Fisher Scientific, France). Cells were maintained at 37 °C in a humidified incubator with 5% CO_2. Subculturing was performed every 2–3 days at ~70% confluency, following PBS wash and treatment with trypsin solution (Thermo Fisher Scientific, France), incubated for 5 min at 37 °C. Trypsin was neutralized with complete medium.

Stimulation: Cells at 70% confluency were serum-starved to minimize background signaling associated with proliferation induced by FBS supplements. Subsequently, cells were stimulated with an FBS-containing medium to activate the MAPK pathway. As controls, only serum-starved cells and cells subjected to 1-hour amino acid starvation were used.

b) *Jurkat cells*

Jurkat T lymphocyte cells are a model of human-T cells.
Culture conditions: RPMI 1640 medium (Thermo Fisher Scientific, France) completed with 10% FBS (Dutscher, France), 1% penicillin-streptomycin (Thermo Fisher Scientific, France) and maintained at 37°C in a humidified incubator with 5% CO2.
In order to maintain exponential growth conditions, the cell density is maintained at around 1 million cells/ml and the medium has been changed/ added every 2 days.

Stimulation was performed using OKT3, a monoclonal antibody targeting human CD3 (Invitrogen, Cat. No. 14-0037-82). After washing the cells with cold PBS, 2 µg of OKT3 was added per 4×10^6 cells and incubated for 20 minutes at 4 °C. Following centrifugation, the supernatant was discarded, and 10 µg of donkey anti-mouse crosslinker (Jackson ImmunoResearch, Cat. No. 715-006-150), which binds the univariable part of the OKT3 antibody, was added. Subsequently, 100 µL of pre-warmed Panserin medium was added per condition, and cells were incubated for stimulation time at 37 °C.
Positive control was cell stimulation with CD3/CD28 beads in a ratio of 2:1 (Dynabeads Human T-Activator CD3/CD28 for T Cell Expansion and Activation, cat. No. 11131D).

c) *B lymphoblastoid cell lines*

B lymphocytes were immortalized by the VVTG platform of the "Necker Enfants Malades" Institute (INEM) using Epstein-Barr Virus (EBV), to generate B-lymphoblastoid (B-LCL) cell lines.

Immortalized B cells are obtained from peripheral blood mononuclear cells (PBMCs) isolated by ficoll from the blood of healthy donors via the Etablissement Français du Sans (EFS)- convention # 2022-2026-046 CCPSL IMAGINE.
Culture conditions: RPMI 1640 medium (Thermo Fisher Scientific, France) supplemented with 10% FBS (Dutscher, France), 1% penicillin-streptomycin (ThermoFischer Scientific, France) at 37°C in a humidified atmosphere with 5% CO2. After several weeks, immortalized B-LCL clones were established and expanded.

B cells were stimulated via BCR by incubation with $F(ab')_2$ Fragment Goat Anti-Human IgM antibody (Jackson ImmunoResearch Laboratories, Cat. No. 109-006-129) for 15 minutes at 37°C. To serve as a positive control for signaling activation, cells were also treated with a combination of phorbol 12-myristate 13-acetate (PMA, Sigma-Aldrich, Cat. No. P8139) and ionomycin (Sigma-Aldrich, Cat. No. I0634). PMA is a phorbol ester that mimics diacylglycerol (DAG), activating protein kinase C (PKC), a key player in signal transduction downstream of BCR engagement. Ionomycin is a calcium ionophore that induces intracellular calcium release, further enhancing signaling pathways. Cells were incubated for 30 minutes with a solution containing 10 ng/mL PMA and 0.5 µg/mL ionomycin to induce robust activation of the BCR signaling cascade, including downstream effectors such as ERK.

PLASMIDS

The coding sequence of *RASAL3* (Ensembl gene ID: ENSG00000105122.13; transcript ID: ENST00000343625.12; length: 3266 bp) was amplified using Q5 High-Fidelity DNA Polymerase (New England Biolabs, Cat. No. M0491S) with primers specifically designed to amplify consecutive exons covering the full-length cDNA (Table 1). The cDNA template was derived from B-LCL of a healthy donor.

Exon targeted	**Primer sequence 5'→3'**	**Direction**	**Location**
Exons 3-4	ACCTCTCCGCTGACTTCCTA	Forward	46-68
	CCCTCGCTCGATATTCCGTC	Reverse	561-580
Exons 4-8	TGCTTGGAGGAGAGGAGGAG	Forward	446-465
	ACGAAGCGAAGGGGCTTC	Reverse	932-949
Exon 9	CCATGCAATGCTTCCTGGAC	Forward	773-792
	TCACCTTCCACTATGCGCG	Reverse	1316-1334
Exons 9-11	CGCTGGAGGAGCTGGAC	Forward	1157-1173
	GGCATCGTGTTCTCAAGCTG	Reverse	1741-1760
Exons 12-13	TCACCTTCCACTATGCGCG	Forward	1612-1631
	GGCATCGTGTTCTCAAGCTG	Reverse	2168-2187
Exon 14	CCATGCAATGCTTCCTGGAC	Forward	2021-2040
	CAAGACCGAAACCAGGCACT	Reverse	2626-2645
Exon 14-end	CGACCCAAAGGCTCCCTGA	Forward	2509-2527

Table 1: Primer sequences used for the amplification of RASAL3 coding sequence (cDNA).
The table lists the primers designed to amplify specific exons of the RASAL3 gene. Each primer is identified by the targeted exon, its sequence (5′→3′), and its direction (forward or reverse). All of them exhibit a melting temperature of around 62 °C, based on their sequence lengths.

The recipient pCMV-HA plasmid was digested with NotI-HF and SalI-HF restriction enzymes. Primers were designed with 5′ overhangs complementary to the plasmid's flanking regions, enabling insertion via the NEBuilder HiFi DNA Assembly Cloning Kit (New England Biolabs, Cat. No. E5520S). The resulting plasmid was transformed into chemically competent E. coli cells (NEB, Cat. No. C2987), which were first cultured in LB medium for 1 hour at 37 °C to allow recovery, and then plated on LB-agar containing ampicillin for overnight incubation at 37 °C.

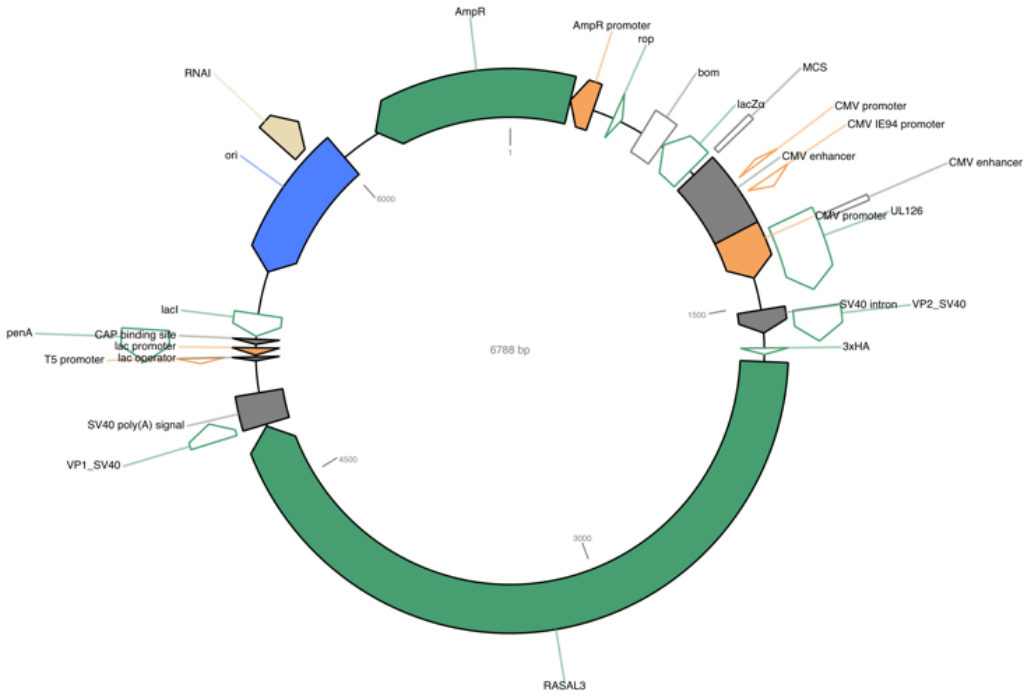

Figure 7: Graphical representation of pCMV-HA-RASAL3 sequence

Colonies carrying the insertion of interest were initially screened by PCR using GoTaq DNA Polymerase (Promega, Cat. No. M3005), following the manufacturer's instructions. The correctness of the insertion was subsequently confirmed by colony PCR followed by Sanger sequencing (3500 Series Genetic Analyzer; Applied Biosystems, Thermo Fisher Scientific) and Oxford Nanopore sequencing (MinION; Oxford Nanopore Technologies, Oxford, UK).

Transfection

HEK cells were seeded in a 12-well plate (300,000 cells per condition) and transfected at 70–80% confluency (1 day after).

The plasmid DNA was diluted in 100 µL of Opti-MEM Reduced Serum Medium (Thermo Fisher Scientific, Cat. No. 31985062) and mixed with 2 µL of Lipofectamine 3000 reagent (Thermo Fisher Scientific, Cat. No. L3000001). The mixture was incubated for 20 minutes at room temperature to allow complex formation. Subsequently, the DNA-lipid complexes were added to cells resuspended in DMEM without serum. After 6 hours of incubation, complete DMEM-containing serum was added to the culture.

To assess transfection efficiency, pCMV-HA-*RASAL3* was co-transfected with a GFP-expressing plasmid at a 10% ratio. The number of cells expressing GFP was quantified using a Penteon flow cytometer (Beckman Coulter)**.** GFP was excited using the 488 nm blue laser**,** and emission was detected through the FITC-A channel, equipped with a 530/30 bandpass filter (detecting fluorescence between 515 and 545 nm).

WESTERN BLOT

Proteins were extracted using RIPA buffer (Thermo Fisher Scientific, Cat. No #89901) supplemented with Halt Protease and Phosphatase Inhibitor Cocktail (100X, ThermoFisher). Equal amounts of proteins were loaded onto 8% NuPAGE Bis-Tris Midi Protein Gels (1.0 mm; Thermo Fisher Scientific, Cat. No. WG1402BOX) and separated using MOPS running buffer. The gel has been transferred onto a PVDF membrane that has been blocked with 5% BSA in a TBS-Tween solution. It was incubated with the primary antibody (dilution 1:1000) overnight at 4°C, followed by 1 hour of washes then 1-hour incubation with corresponding secondary antibody incubation (dilution 1:10000).
Detection was performed using SuperSignal West Pico PLUS (Thermo Fisher Scientific) or Atto ECL solutions (Thermo Fisher Scientific, Cat. No #A38556), according to the manufacturer's instructions. Chemiluminescent signals were visualized using the Fusion imaging system.
The antibodies used to detect different targets are:

Target Protein	**Antibody Type**	**Host species**	**Supplier**	**Catalog Number**	**Expected size**	**Dilution**
AKT	Primary	Mouse	CST	2029S	60 kDa	1:1000
Anti-Rabbit	Secondary	Goat	CST	7074S	-	1:10000
Anti-Mouse	Secondary	Horse	CST	7076S	-	1:10000
ERK 1/2	Primary	Rabbit	CST	9101	42-44 kDa	1:1000
GAPDH	Primary	Rabbit	CST	2118S	37 kDa	1:1000
Ku70	Primary	Rabbit	CST	4588	70 kDa	1:1000
HA-tag	Primary	Mouse	CST	2367S	-	1:1000
pAKT (Ser473)	Primary	Rabbit	CST	4060	60 kDa	1:1000
pERK (Thr202/Tyr204)	Primary	Rabbit	CST	9102	42-44 kDa	1:1000

pS6RP (Ser240/244)	Primary	Rabbit	CST	5364	32 kDa	1:1000
RASAL3	Primary	Rabbit	Proteintech	21164-1-AP	112 kDa	1:1000
S6RP	Primary	Mouse	CST	2317	32 kDa	1:1000

Table 2: List of antibodies used for Western blot

The detection of phosphorylated forms of each target and the total protein levels was performed on the same membrane. After detecting the phosphorylated proteins, the membrane was stripped using Restore Western Blot Stripping Buffer (Thermo Fisher Scientific, Cat. No. 21059) according to the manufacturer's protocol. Briefly, the membrane was incubated in the stripping buffer for 30 minutes at room temperature with gentle agitation, then washed thoroughly in TBS-Tween before proceeding with re-blocking and re-probing for total protein levels.

CYTOMETRY ASSAY

Detection of phosphorylated ERK was detected by flow cytometry using the PerFix EXPOSE Kit (Beckman Coulter, Cat. No. B31167) according to the manufacturer's instructions. Briefly, after stimulation, 200.000 cells are fixed and permeabilized, then stained with a fluorochrome-conjugated antibody targeting intracellular phopho-epitopes (BioLegend Brilliant Violet 421 anti-ERK1/2 Phospho (Thr202/Tyr204) Antibody, Cat. No. 369509). Samples were acquired using a NovoCyte Penteon Flow Cytometer (Agilent, France), and data were analyzed with FlowJo software (BD Biosciences).

The negative control were non stimulated cells and the positive control was cell stimulation with CD3/CD28 beads at ratio 2:1 (Dynabeads Human T-Activator CD3/CD28 for T Cell Expansion and Activation, cat. No. 11131D). The combination of CD3 and CD28 beads replicates the physiological condition of TCR activation.

Lymphocytes were gated based on FSC/SSC to select lymphocytes. To exclude doublets, singlet gating was performed by plotting FSC-H versus FSC-A, and only events along the diagonal were included in the analysis. In addition, the non-stimulated (NS) condition was used as a baseline reference to define the background level of fluorescence, against which pERK induction in stimulated cells was measured.

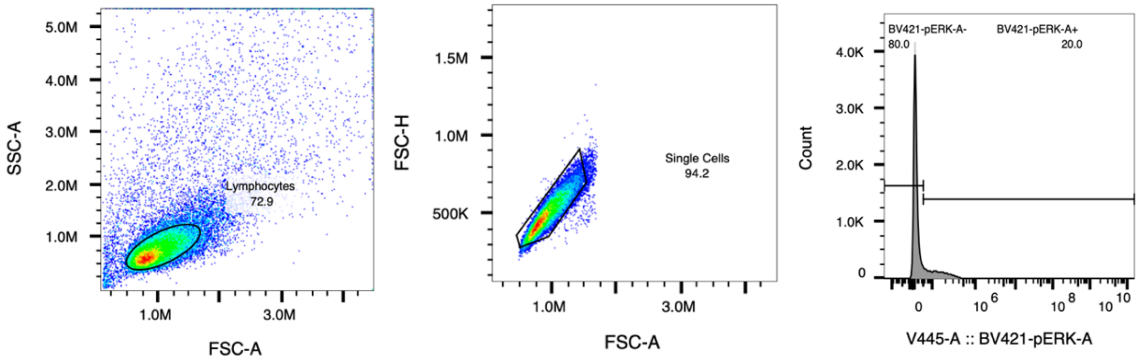

Figure 8: Gating strategy for the FACS analysis of pERK expression assessment. To ensure the validity of the analysis, it has been selected lymphocyte population based on size and granularity and doublets have been excluded. The measure of

positives cells detected in non-stimulated condition has been considered as baseline level of pERK, not correlated with stimulation.

Site-Directed Mutagenesis

Point mutations were introduced into pCMV-HA-*RASAL3* plasmid using the NEBuilder HiFi DNA Assembly protocol. The design of primers has been done through the NEBuilder tool. Primers specific for each variant were designed using the NEBaseChanger tool. The annealing temperatures for each primer pair are listed below:

Mutation	Forward primer	Reverse primer	Temp. Annealing
c.418T>C	CATTGGGGGCCTCACCCTGCT	TCCCAGACAGGCACGTTG	65°C
c.856G>A	CCGCTGGATCAAGGACCTTCG	TCTCTCTCAGCGGCCGAG	71°C
c.2312C>T	GGCTTCCTGGTCCCCCGGAC	GGGCTTCTCCCCTGCGGAG	72°C
c.1936C>T	CAAGGTCATCTAGAACCTCGC	GCAATCAGTGTGAGGGTG	64°C
c.1588C>T	ACAGGTTGTGTGGCGTCTCTG	CCCAGGGTCTCCTGGAGG	71°C

Table 3: The sequences of the primers specific for each mutation, that has been designed with NEBaseChanger tool with the corresponding temperature of annealing.

The mutations were generated by Q5 Hot Start PCR on pCMV-HA-*RASAL3* WT plasmid, by using the primers designed. The condition of the thermocycler was settled following the manufacturer's guidelines, where the temperature of annealing is defined by the primers used and the time of elongation depends on the length of the construction (for pCMV-HA-*RASAL3* is 6788bp):

STEP	TEMP	TIME
Initial Denaturation	98°C	00:30
30 cycles	98°C	00:10
Final extension	Temp. annealing of the selected primers	03: 30
Hold	4°C	∞

Table 4: Thermocycler setting for PCR reaction for DNA of pCMV -HA-RASAL3 WT

To optimize PCR conditions in cases where inefficient amplification was observed, due to suboptimal primer annealing temperatures, a gradient PCR was performed using Q5 High-Fidelity DNA Polymerase on the Smart Gradient PCR Thermal

Cycler T960. This approach allowed for the identification of the optimal annealing temperature to improve specificity and yield.
The PCR product was analyzed by agarose gel electrophoresis compared with a 1Kbp DNA ladder.
The PCR product is ligated through KLD Enzyme Mix Reaction Protocol (NEB #M0554).
E. coli NEB 5-alpha (NEB #C2987) cells were transformed with the assembly product and incubated first in LB medium for 1 hour at 37 °C to allow recovery, and then plated on LB-agar containing ampicillin for overnight incubation at 37 °C.

Randomly colonies on the selection plate have been chosen in order to perform Promega GoTaq DNA Polymerase by using primers located on exons closed to the mutation of interest. The colonies that show the expected band when analyzed by agarose gel electrophoresis have been sequenced with 3500 Series Genetic Analyzer (Applied Biosystems, Thermo Fisher Scientific) by using BigDye Terminator v3.1 Cycle Sequencing Kit and the primer of the closed exon. The sequencing electropherogram showing the expected mutation, with no additional mismatches when aligned to the wild-type *RASAL3* sequence, was selected for following analyses. Subsequent nanopore sequencing analysis confirmed the presence and integrity of the expected mutation, with no additional sequence alterations detected.

pLVX-HA-RASAL3 construction

The construction of the plasmid was performed first in silico through NEBBuilder tool in order to select the couple of digestion plasmids and primers for the amplification of *RASAL3* sequence from pCMV-HA-*RASAL3* template.
The digestion enzymes chosen (BamHi-HF and EcoRI-HF) were compatible for the temperature of activity and buffer of reaction (rCutSmart Buffer**).**

Component Fragments

Name	Length	Produced by	5' End	3' End
HA-RASAL3 WT	3133	PCR	Fwd Primer (auto)	Rev Primer (auto)
PLVX	8868	Restriction Digest	BamHI-HF	EcoRI-HF

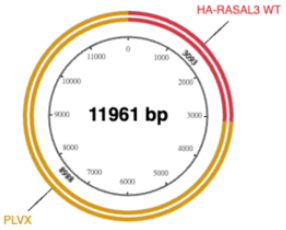

Primers	Sequence	Tm
HA-*RASAL3* WT Fwd	gtgaggatctatttccggtgATGTACCCATACGATGTTCC	62°C
HA-*RASAL3* WT Rev	gggggagggagaggggcggTCAGGTGGTGTCTCCATTG	62°C

Figure 9: Summary of the in-silico plasmid construction and table of primers for amplification of RASAL3 insert generated in order to match with the compatible ends of the digested plasmid (the sequence in uppercase is the annealing part).

The digested plasmid and the amplified insert were assembled following the indication of NEBuilder HiFi DNA Assembly Mix.
The NEB Stable Competent E.Coli (High efficiency) C3040 was transformed with the assembled plasmid in order to obtain multiple copies of the plasmid of interest. The colonies carrying the correct plasmid have been identified through gel agarose 1%, Sanger sequencing and Nanopore sequencing.

RESULTS

Description of the identified RASAL3 variants

As part of the genetic analysis, WES was performed on patients affected by pediatric autoimmune diseases from multiple ongoing research projects. This analysis revealed 5 variants with high deleteriousness and pathogenicity, all affecting the same gene: *RASAL3*. Additionally, two patients show possible pathogenic variants in other genes, including PLCG2, RASA1 and ABCB4[3].

For each variant, several predictive tools and population databases were utilized. In particular, gnomAD (Genome Aggregation Database), an informatic resource that aggregates and harmonizes exome and genome sequencing data from large-scale sequencing projects, was used to assess the frequency across different zygosity states in the general population. GnomAD provides an insight into the potential pathogenicity of a variant; for example, a variant that is relatively common in the heterozygous state but rare or absent in the homozygous state may suggest that homozygosity is not well tolerated, potentially due to deleterious effects (Table 5). Given the established role of RASAL3 in regulating T and B lymphocyte activation, the primary objective of this study is to evaluate the impact of these mutations on the associated signaling pathways.

Patient N.	CDS position	Protein position	GnomAD n/Hzm	CADD	Polyphen	SIFT	Zygosity	*Phenotype*	Other potentially causative variants
1	c.418T>C	p.F140L	1/0	25.9	0.958	0.01	Heterozyous	AIH	PLCG2
2	c.856G>A	p.E286K	0/0	25.8	0.723	0	Heterozygous	AIH	RASA1 ABCB4
3	c.1588C>T	p.R530W	9/0	25	0.761	0.02	Heterozygous	Evans syndrome	
4	c.1936C>T	p.Q646*	1/0	41	-	-	Heterozygous	Evans syndrome	
5	c.2312C>T	p.A771V	3/0	23.7	0.16	0.01	Heterozygous	AIH	

Table 5: Summary of genetic variants identified in the patient cohort.
The table presents information on variant type, disease of the patient (AIH for autoimmune hepatitis) predicted effect, and population frequency: GnomAD (ratio of heterozygous cases and homozygous ones in the all population); CADD (predictive score that estimates the deleteriousness of the variant, a value above 20 indicates that the variant is among the top 1% most deleterious variants in the human genome); Polyphen (evaluates the potential impact of an amino acid substitution on the structure and function of a protein, a value of 0 corresponds to

[3] PLCG2 (Phospholipase C Gamma 2) (https://www.ncbi.nlm.nih.gov/gene/533); RASA1 (RAS p21 Protein Activator 1) (https://www.ncbi.nlm.nih.gov/gene/5921); ABCB4 (ATP Binding Cassette Subfamily B Member 4) (https://www.ncbi.nlm.nih.gov/gene/5244).

a benign mutation); SIFT (it predicts whether a missense variant is likely to affect protein function, a score below 0.05 suggests a potentially deleterious effect).

The median age at diagnosis within the cohort was 6 years. Among the three patients diagnosed with AIH, two were classified as having type II AIH.

- Patient 1 (mutation c.418C>T): the predominant clinical manifestation is type 1 diabetes mellitus.
- Patient 2 (mutation c.856C>T): clinical features include neonatal jaundice and pyelonephritis.
- Patient 3 (mutation c.2312C>T): this patient presented with inflammatory bowel disease (IBD), sclerosing cholangitis, and recurrent seromucous ear infections
- ES case: clinical data were available for only one patient, who presented with neutropenia, thrombocytopenia, and autoantibodies against IgG, C3d, and CD16. The patient was undergoing immunosuppressive treatment with sirolimus.

The patients included in this study were diagnosed with either autoimmune hepatitis or Evans syndrome. The five RASAL3 variants under investigation were distributed across different regions of the coding sequence, with some located in the pleckstrin homology (PH) domain and others within the catalytic domain. All were missense mutations, with the exception of one truncating variant (Fig.10).

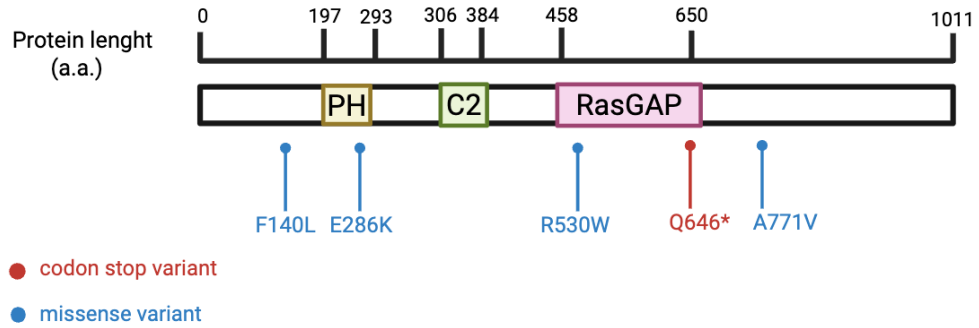

Figure 10: Schematic representation of RASAL3 protein sequence showing the position and type of the variants analyzed in this study. Each variant is indicated along the coding sequence according to its protein position, and categorized based on its predicted molecular consequence (e.g., missense mutation or stop codon gain)

Setting up of the standard experimental condition

Clearly defining experimental conditions is essential to ensure the reproducibility, reliability, and interpretability of our findings. To this end, we established carefully controlled and standardized conditions to investigate the role of RASAL3 in the selected in vitro models. This rigorous approach strengthens the validity of our experimental design and the conclusions drawn from the data.

Given that RASAL3 may participate in different signaling cascades ultimately leading to ERK phosphorylation, we evaluated pERK induction following TCR

stimulation in T cells, BCR stimulation in B cells, and growth factor stimulation in HEK cell lines.

1. Phospho-ERK expression in Jurkat T cells after stimulation by OKT3

The determination of the optimal concentration for OKT3 monoclonal antibody for inducing TCR-mediated signaling in Jurkat cells was done to maxime assay reproducibility while replicating physiological conditions. Insufficient antibody concentrations fail to initiate downstream signaling, whereas excessive levels can result in hyperactivation and non-physiological cellular responses.
To identify the appropriate stimulation conditions, we tested a range of OKT3 concentrations (10µgr/ml; 1µgr/ml; 0,5µgr/ml; 0,1µgr/ml), keeping cell density and stimulation time (15 minutes) constant across all conditions (Fig. 11B).

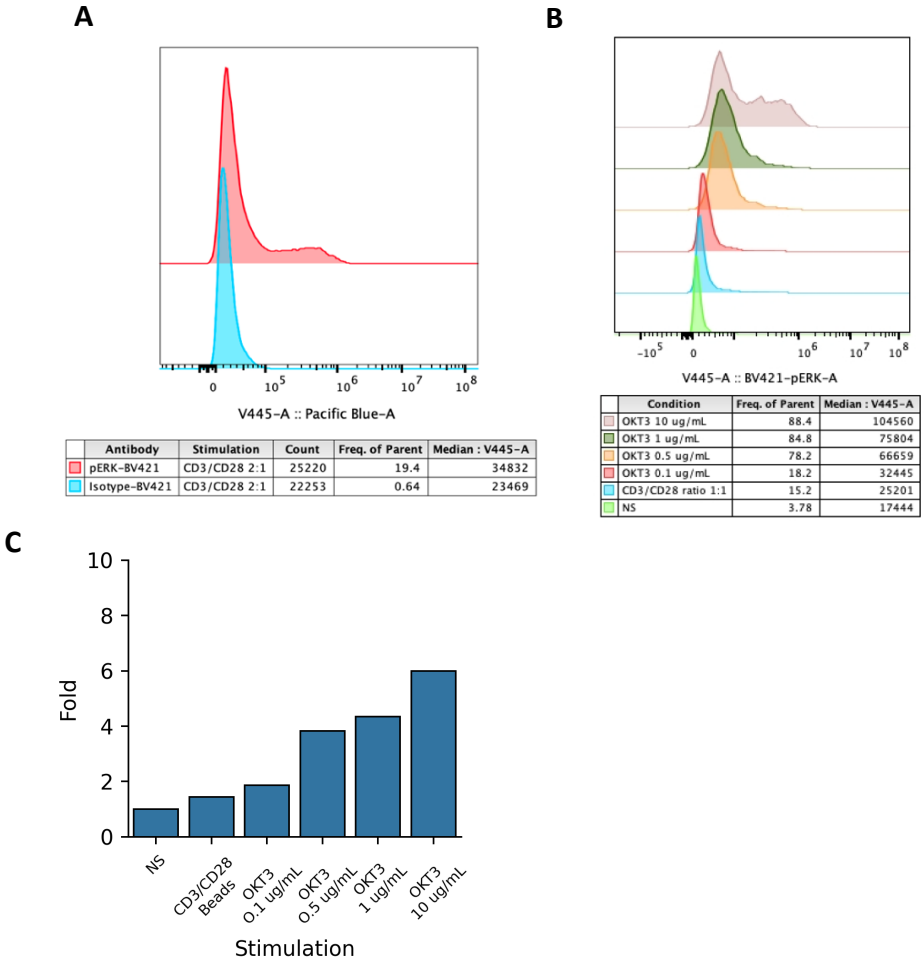

Antibody	Stimulation	Count	Freq. of Parent	Median : V445-A
pERK-BV421	CD3/CD28 2:1	25220	19.4	34832
Isotype-BV421	CD3/CD28 2:1	22253	0.64	23469

Condition	Freq. of Parent	Median : V445-A
OKT3 10 ug/mL	88.4	104560
OKT3 1 ug/mL	84.8	75804
OKT3 0.5 ug/mL	78.2	66659
OKT3 0.1 ug/mL	18.2	32445
CD3/CD28 ratio 1:1	15.2	25201
NS	3.78	17444

Figure 11: FACS analysis of pERK expression in Jurkat T cells. The x axis represents the intensity of fluorescence of the pERK; the y axis represents the number of cells.
(A) represents the signal obtained with CD3 and CD28 beads (ratio 2:1) and using Violet 421 anti-ERK1/2 Phospho (Thr202/Tyr204) Antibody or isotype-BV421 antibody, assessing the absence of unspecified signal.
(B) pERK expression was assessed after different conditions of stimulation.

(C) Graphical representation of pERK expression induction (log fold change) for each condition as compared to unstimulated condition.

Background fluorescence and non-specific antibody binding were evaluated by comparing the pERK signal in cells stimulated with CD3/CD28 beads using either the pERK antibody or an isotype control. The absence of a detectable pERK signal in the isotype control confirmed the specificity of the staining and indicated minimal non-specific binding (Fig.11A).
Flow cytometry analysis of pERK levels following TCR stimulation with varying concentrations of OKT3 antibody demonstrates a dose-dependent increase in ERK phosphorylation. As shown in the overlaid histogram (Fig. 11B), all stimulated conditions exhibit a rightward shift in fluorescence intensity (BV421-A channel) compared to the non-stimulated (NS) control, indicating increasing pERK levels.
The optimal concertation of OKT3 for robust pERK induction is 1µgr/ml for 200.000 cells.
In contrast, stimulation with CD3/CD28 beads did not result in significant activation of the TCR signaling cascade, as evidenced by low pERK expression (Fig.11C). This lack of response may be attributed to suboptimal beads ratio, insufficient stimulation duration, or potentially low CD28 expression levels in the Jurkat cell line used.

2. Phospho-ERK expression in B-LCL after stimulation by anti-IgM

To validate the protocol for pERK induction in B cells, B-LCLs generated from a healthy donor were used. pERK levels were assessed using both flow cytometry (Fig. 12A) and Western Blot (Fig.12B).

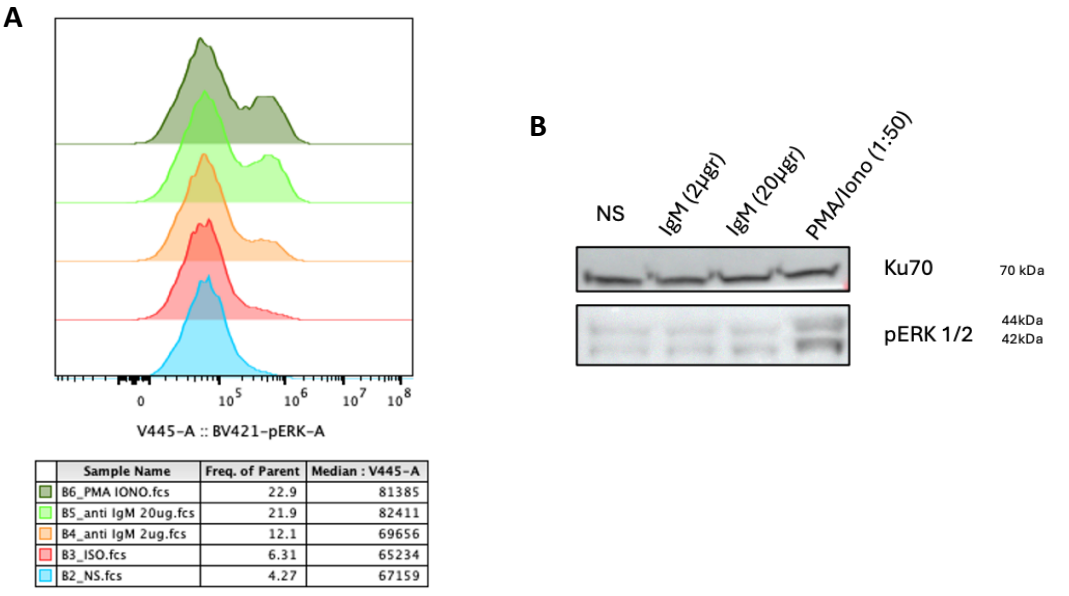

	Sample Name	Freq. of Parent	Median : V445-A
	B6_PMA IONO.fcs	22.9	81385
	B5_anti IgM 20ug.fcs	21.9	82411
	B4_anti IgM 2ug.fcs	12.1	69656
	B3_ISO.fcs	6.31	65234
	B2_NS.fcs	4.27	67159

Figure 12: pERK detection in B-LCL under different stimulation conditions: PMA/ionomycin (PMA-IONO) as a positive control, anti-IgM antibody stimulation at two concentrations, and non-stimulated cells (NS).
(A) Flow cytometry analysis of levels of pERK in B-LCL for each condition.
(B) Western blot analysis of pERK expression in the same conditions. Ku70 was used as a loading control.

Non-stimulated controls, two different concentrations of anti-IgM antibody, and PMA/ionomycin (PMA-IONO) as a positive control were tested. In the flow cytometry assay, the isotype control confirmed the absence of non-specific staining. Anti-IgM stimulation effectively induced ERK phosphorylation in a dose-dependent manner, as shown in Fig. 12A. Notably, stimulation with 20 ngr of anti-IgM resulted in pERK levels comparable to the positive control, with a frequency of pERK-positive cells around 22%.
The protein extracted from the same conditions were then analyzed by Western blot (Fig.12B). However, pERK was not detectable using this technique: these results suggest that flow cytometry provides higher sensitivity for detecting pERK under these experimental conditions.

It is important to interpret these findings with caution, as the anti-IgM antibody used for stimulation had been stored for an extended period, potentially reducing its efficacy and compromising the reliability of the observed effects. Nevertheless, ERK phosphorylation in response to anti-IgM was clearly detectable by flow cytometry (Fig. 12).

3. Phospho-ERK expression in HEK after serum stimulation

To further investigate signaling pathways potentially regulated by RASAL3, we utilized HEK293 cells and evaluated the phosphorylation of key intracellular targets following serum stimulation. Cells were serum-starved prior to stimulation, and four time points were tested: 5, 10, 15, and 30 minutes (Fig. 13).

The goal was to identify the optimal stimulation duration capable of inducing phosphorylation of the proteins of interest.

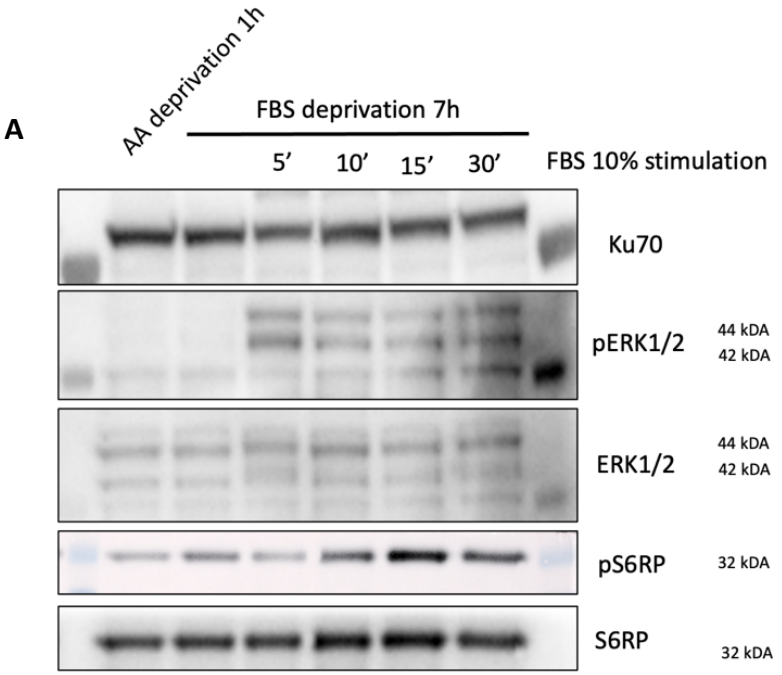

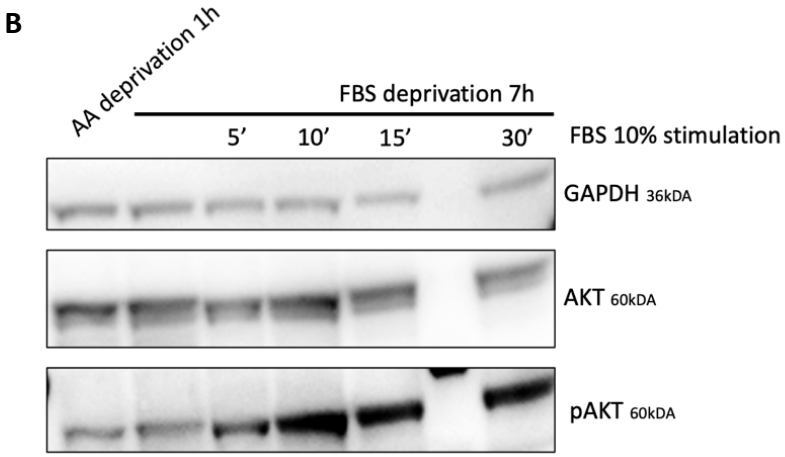

Figure 13: Western blot analysis of phosphorylated and total forms of ERK, AKT, and S6RP in HEK cells under different culture conditions.
HEK cells were subjected to amino acid (AA) deprivation for 1 hour, serum (FBS) starvation for 7 hours, or FBS starvation followed by re-stimulation with complete medium for defined time points (5, 10, and 15 minutes). Phosphorylated and total levels of ERK, AKT, and S6RP were analysed. GAPDH and Ku70 are the housekeeping genes used to confirm the equal total amount of protein loaded.

Both 7-hour FBS starvation and 1-hour amino acid (AA) deprivation successfully abolished detectable pERK levels, confirming suppression of basal pathway activation.

Three bands were detected with the anti-ERK antibody; however, only the two upper bands corresponded to ERK1 and ERK2 isoforms, which are directly involved in MAPK signaling. The lower band likely represents non-specific binding. pERK peaked at 5 minutes post-stimulation, consistent with the rapid and transient nature of ERK activation. It decreased at later time points. Total ERK levels remained constant, suggesting that stimulation modulates protein activation rather than synthesis (Fig.13A).

In contrast, phosphorylation of S6RP was not significantly induced at the 5-minute mark, indicating that longer stimulation is required for its activation. This delay may reflect its downstream position in the signaling cascade relative to ERK. A similar trend was observed for AKT, for which phosphorylation also required a longer stimulation period. Importantly, no de novo protein synthesis was observed for either S6RP or AKT (Fig.13A-B).
These results indicated that serum stimulation efficiently activates ERK within 5 minutes, while downstream targets such as AKT and S6RP reach maximal phosphorylation after 10 minutes.

In addition, different starvation durations were tested to determine the minimal time required to suppress basal pathway activity.

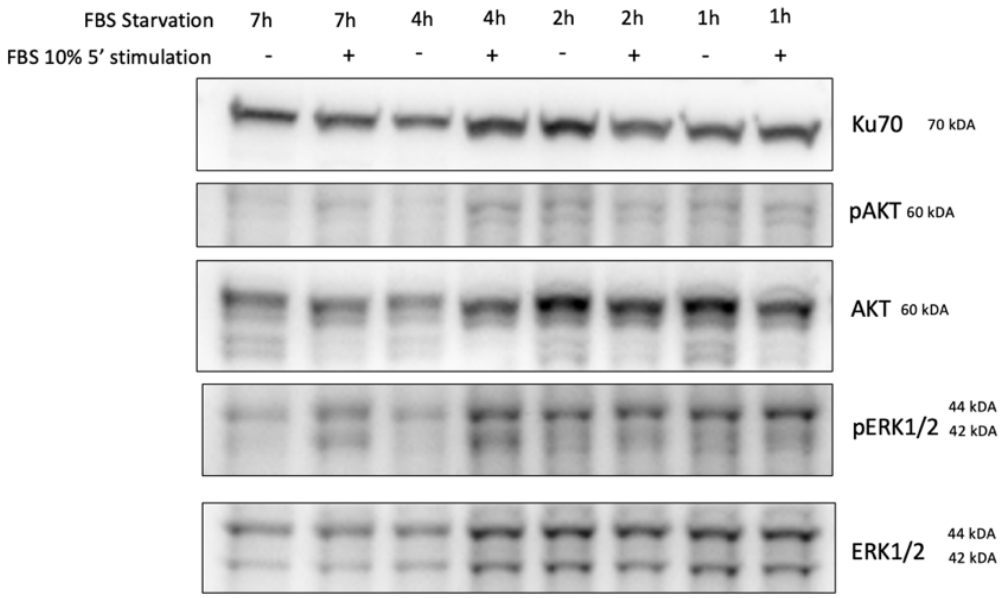

Figure 14: Western blot analysis of HEK cells subjected to different durations of serum starvation followed by stimulation with FBS for 5 minutes. For each time point, both unstimulated and FBS-stimulated conditions are shown. Ku70 was used as a loading control to confirm equal protein loading across samples.

When cells were starved for two hours or less, no clear difference was observed between stimulated and unstimulated conditions. While four hours of starvation did reduce basal phosphorylation, pERK levels were still higher than after seven hours, suggesting incomplete suppression.

In conclusion, a starvation period of at least four hours is required to effectively reduce baseline signaling and enhance the responsiveness of HEK cells to serum stimulation (Fig. 14).

4. Transfection efficiency

To ensure reproducibility and avoid non-specific effects or cytotoxic responses, it is crucial to determine the minimal effective dose of plasmid DNA required for transfection. Excessive plasmid concentrations can impose a metabolic burden and result in overexpression of the target protein**,** potentially leading to deleterious effects on HEK cells.

This use of the lowest plasmid concentration that ensures efficient transfection while preserving cell viability and minimizing experimental artifacts associated with overexpression.
The adopted optimization strategy was based on HEK cells analysis by flow cytometry: HEK cells were transfected with increasing amounts of the pCMV-HA-RASAL3 plasmid co-transfected with GFP (ratios: 100:10, 200:20, 500:50, 1000:100). The frequency of GFP-positive cells served as an indirect marker of transfection efficiency (Fig. 15)

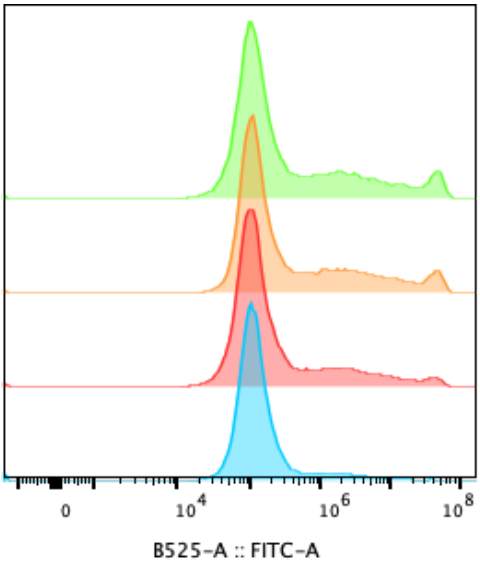

	Sample Name	Freq. of Parent	Count
	A8_RASAL3 1000.fcs	36.6	52995
	A7_RASAL3 500.fcs	37.0	45884
	A6_RASAL3 200.fcs	28.3	49584
	A5_RASAL3 100.fcs	15.1	43792

Figure 15: Flow cytometry analysis of transfected HEK cells with different amounts of plasmid pCMV-HA-RASAL3 and GFP (100:10; 200:20; 500:50; 1000:100). The proportion of GFP-positive cells was used as an indirect measure of transfection efficiency. Given the fixed co-transfection ratio, GFP expression was considered indicative of successful uptake and expression of the RASAL3-encoding plasmid.

Optimal transfection efficiency is generally expected to approach 70%, ensuring a balance between high expression and minimal cellular stress. However, in this experiment, the efficiency ranged between 30% and 40%, which is below the desired threshold (Fig. 15). This suggests that further optimization—potentially involving alternative plasmid concentrations or transfection reagents—is necessary.

To confirm expression of the transfected construct, higher concentrations of pCMV-HA-RASAL3 WT were tested. RASAL3 protein expression was successfully detected by Western blot using both anti-RASAL3 and anti-HA tag antibodies.

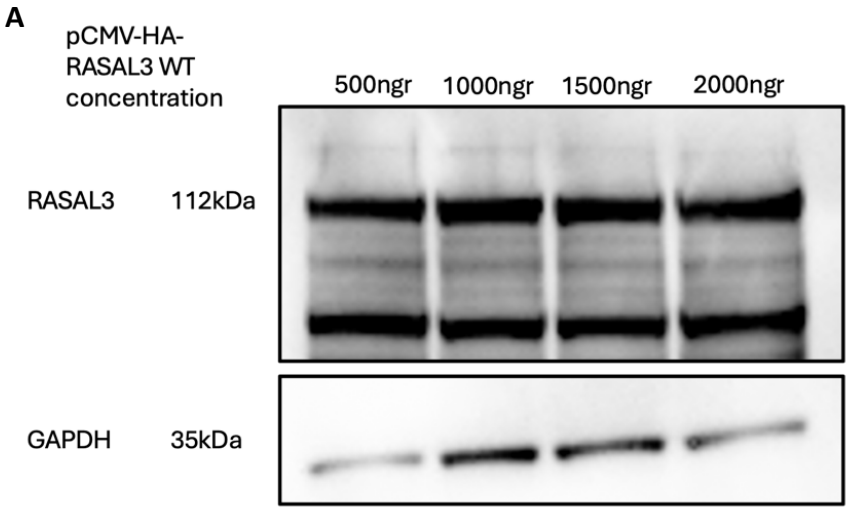

B

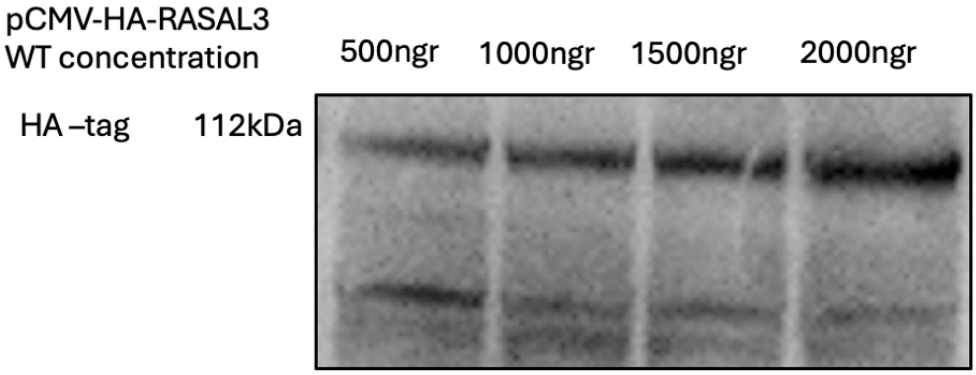

Figure 16: Western blot analysis of HEK cells transfected with different amount of plasmid pCMV-HA-RASAL3 WT (500ngr, 1000ngr, 1500ngr, 2000ngr).
GAPDH is detected as a housekeeping gene to validate the efficient protein dosage.
(A) detection with RASAL3 antibody.
(B) Detection with HA-tag antibody after stripping the membrane.

Western blot analysis revealed strong and consistent expression of RASAL3 at approximately 112 kDa across all tested plasmid concentrations (Fig.16). Detection with both the anti-RASAL3 and anti-HA tag antibodies confirmed that the expressed protein is full-length and HA-tagged. Although signal intensity increased slightly with higher plasmid concentrations, expression was already efficient at 500 ng, suggesting early saturation or high transfection efficiency. GAPDH expression was uniform across samples, supporting the reliability of protein quantification. These findings validate the specificity of both antibodies used.

Transfection of HEK cells with pCMV-HA-RASAL3 WT under these conditions was therefore considered successful and reproducible.

Transfection of HEK cells with pCMV-HA-RASAL3 WT

Based on the optimized conditions previously established, HEK cells were transfected with the pCMV-HA-RASAL3 WT plasmid. Transfection efficiency was evaluated by Western blot analysis using anti-GFP, anti-HA, and anti-RASAL3 antibodies, as reported in Figure 23 (Appendix). The specificity of the anti-RASAL3 antibody was validated by assessing protein expression across multiple cell types.

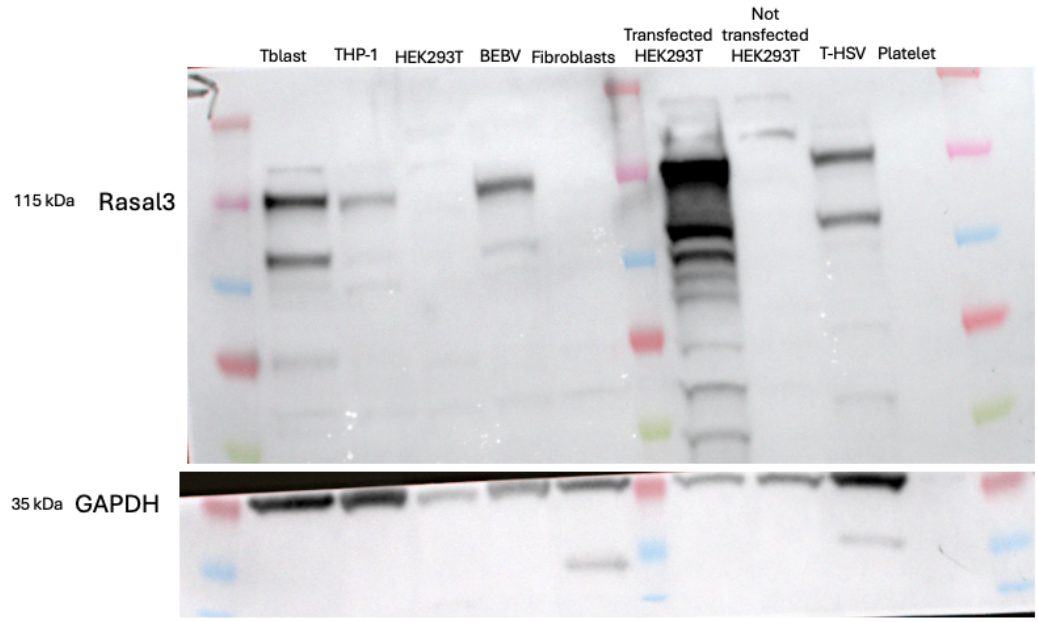

Figure 17: Western blot of lysates from different cell types (Tblast, THP-1, BEBV, Fribroblast, HEK 293 T cells transfected and not, T-HSV, Platelets). Detection of RASAL3 has been performed by incubating the membrane with a specific anitbody (Proteintech 21164-1-AP).

As reported in the literature, RASAL3 is expressed in T cells (T blast), B cells (B-LCL line) and myeloid cell line (THP1), but not in non-transfected HEK cells, fibroblasts, or platelets (Fig.17). These results support the specificity of the anti-RASAL3 antibody and confirm the success of the transfection.

Following transfection, HEK cells showed a distinct band at the expected molecular weight (~115 kDa), indicating successful expression of RASAL3. However, additional non-specific bands of various molecular weights were also observed (Fig.17).

Nonetheless, several limitations must be considered. Variability was observed in the expression of the housekeeping gene GAPDH, which is notably absent in platelets, complicating normalization. Furthermore, the presence of lower molecular weight bands in transfected cells may suggest protein cleavage or post-translational modifications affecting RASAL3 size.

To assess transfection efficiency and antibody specificity, HEK cells transfected with the empty vector or the WT RASAL3 plasmid were compared to non-transfected cells under identical stimulation conditions.

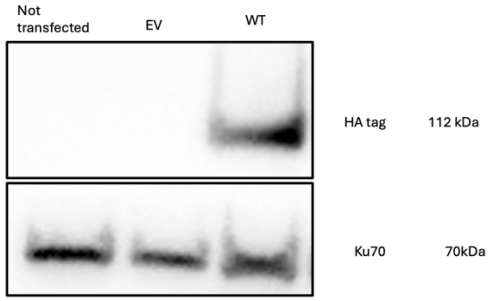

Figure 18: Western blot analysis of lysates from HEK293 cells untransfected, transfected with empty vector (EV), or with pCMV-HA-RASAL3 WT. Blots were probed for HA-tag and the housekeeping protein Ku70 (loading control).

A strong HA signal was observed exclusively in cells transfected with the WT plasmid, confirming both transfection efficiency and the specificity of the anti-HA antibody (fig. 18). Additionally, by directly probing for the HA tag without prior membrane stripping, the previously observed secondary band was no longer detectable, suggesting it was due to non-specific antibody binding rather than true RASAL3 expression or cleavage product.

Site-directed mutagenesis

All RASAL3 point mutations were successfully generated and validated by Sanger sequencing (Fig. 19). Subsequent nanopore sequencing confirmed the presence and integrity of the engineered variants, with no additional sequence alterations detected.

The c.418C>T mutation, however, initially failed to amplify under standard PCR conditions using the predicted annealing temperature for the primer pair (see Table 3). To overcome this, a gradient PCR was performed, and the expected amplification band was successfully detected on a 1% agarose gel at an annealing temperature of approximately 69 °C.

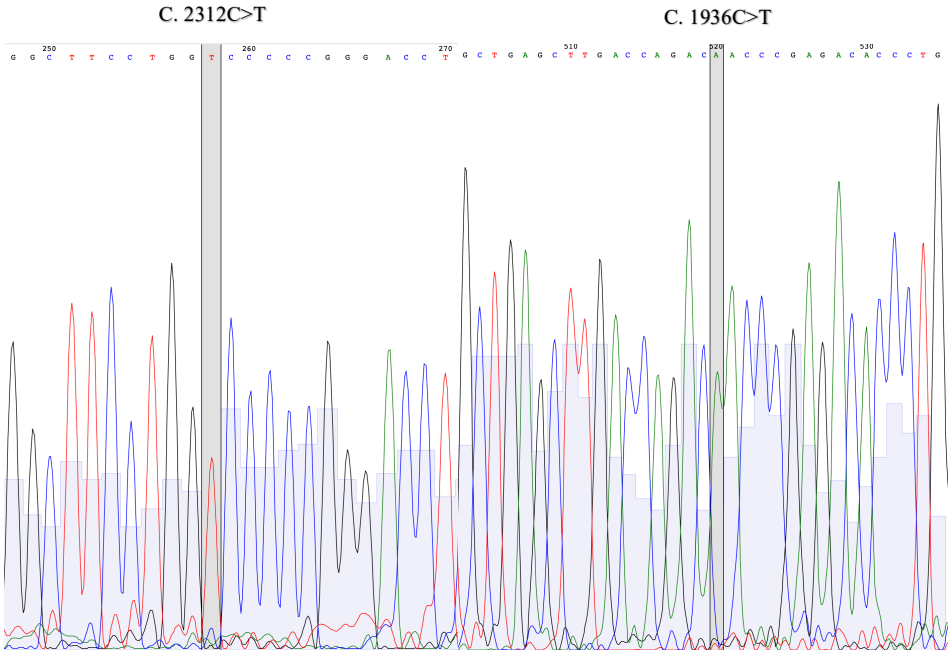

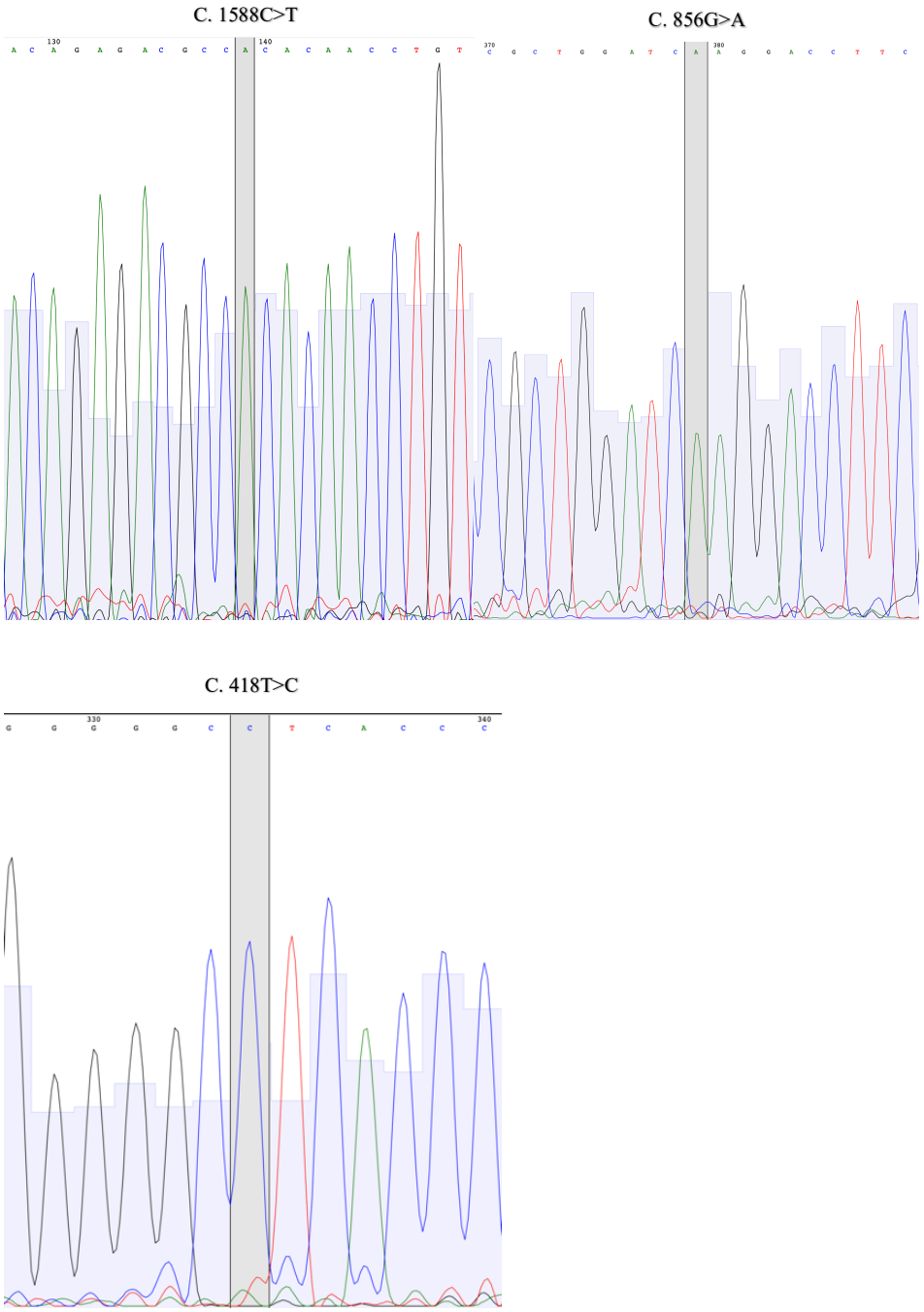

Figure 19: Sanger sequencing chromatograms confirming the presence of the engineered RASAL3 mutations. The grey-shaded regions highlight the nucleotide positions where the expected point mutations were introduced (The sequencing has been performed with Forward primer for some of them and with Reverse primer for others).

All plasmids carrying the different successfully generated mutants were amplified through liquid culture followed by plasmid DNA purification. These plasmids were then used for a primary transfection experiment (see Fig. 24, Appendix).

pLVX-HA-RASAL3-mCherry WT generation

The wild-type RASAL3 coding sequence was successfully cloned into the pLVX-HA-mCherry vector. Following bacterial transformation, twelve colonies were screened by colony PCR using primers specific for the EF1α promoter (located in the plasmid backbone) and exon 2 of RASAL3. Seven colonies showing amplification products of the expected size were selected for further validation by nanopore sequencing (Fig. 20). Among these, two colonies were confirmed to carry the correct RASAL3 sequence.

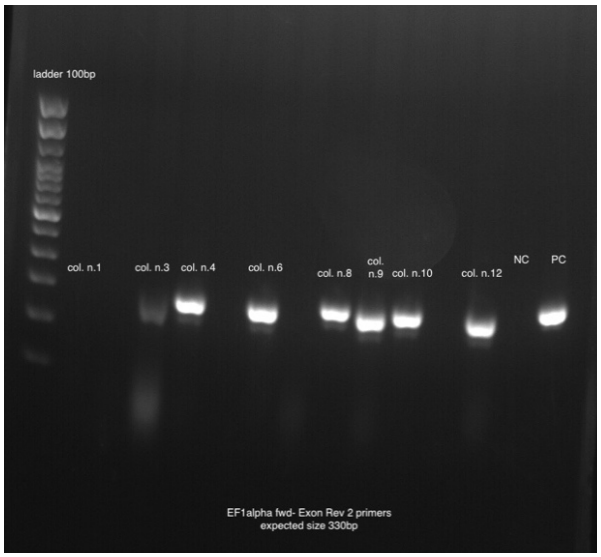

Figure 20: Agarose gel electrophoresis of colony PCR products from 12 randomly selected bacterial colonies transformed with pLVX-HA-RASAL3-mCherry (WT). GoTaq DNA Polymerase was used with primers targeting the EF1α promoter in the plasmid backbone and RASAL3 exon 2. Bands at the expected sizes confirm successful insertion of the RASAL3-mCherry cassette.

The generation of the pLVX plasmids carrying the mutated forms of RASAL3 has not been successfully achieved so far. Two different strategies were tested: (I) site-directed mutagenesis on the pLVX plasmid containing the wild-type RASAL3 coding sequence using previously designed primers (Table 3), and (II) amplification of the mutant RASAL3 sequence from the pCMV plasmid followed by its insertion into the empty pLVX vector, using primers designed for this cloning strategy (figure 20). However, both approaches failed to produce the desired constructs, likely due to suboptimal primers or inappropriate annealing temperatures during PCR amplification.

DISCUSSION

Autoimmune diseases represent a heterogeneous group of conditions characterized by an abnormal immune response against self-antigens. Studying early onset and multi-familial cases provides a unique opportunity to identify new genetic factors impacting lymphocytes homeostasis. Given their early manifestation, it is widely believed that genetic factors play a predominant role in their pathogenesis, highlighting the importance of exploring the genetic landscape in affected children. Studying these variants offers critical insights into the molecular mechanisms underlying immune responses and may help reveal previously unknown regulators of this intricate system. It provides a valuable opportunity to uncover new mechanisms of lymphocytes regulation, to identify diagnostic biomarkers and potential therapeutic targets.

RASAL3, a Ras GTPase-activating protein (RasGAP) expressed in T cells, monocytes and neutrophils, has emerged as a potential regulator of TCR-mediated signaling. While its exact physiological role is not yet fully defined, preliminary evidence suggests that RASAL3 contributes to peripheral T cell survival and homeostasis. Notably, although several RasGAPs exist, *RASAL3* appears to fulfill a non-redundant role in T cells. Deletion of *RASAL3* impairs peripheral T cell survival and disrupts immune homeostasis (Muro et al., 2018; Saito et al., 2015; Saito et al., 2015). The main role of RASAL3 is as a negative regulator of the RAS/MAPK pathway that is a key signaling axis induced after T cell and B cell activation. In particular, the specific receptors located on the membrane of the immune cells (TCR or BCR) recognize the antigen and induce the cellular response specific.

Given the evidence that TCR-mediated activation of the RAS pathway can trigger opposing outcomes, it is reasonable to hypothesize that RASAL3 acts as a molecular switch modulating the amplitude and duration of Ras activity. Through this fine-tuning mechanism, RASAL3 ensures proper signal interpretation and corresponding cellular responses.

In this context, altered RASAL3 function (whether due to loss, gain, or dysregulation) may lead to sustained Ras activation, resulting in hyperactivation of T and B lymphocytes and contributing to immune dysregulation syndromes characterized by autoimmunity and lymphoproliferation. These functional changes could impair immune tolerance mechanisms, promote the survival of autoreactive clones, or enhance inflammatory signaling, ultimately fostering the development of complex autoimmune phenotypes.

The hypothesis that this mechanism may play a role in the pathogenesis of Autoimmune Hepatitis (AIH) and Evans Syndrome (ES) is supported by evidence indicating that both conditions are characterized by immune-mediated tissue damage and dysregulated lymphocyte activity. Some patients also display overlapping features with ALPS, which involves impaired lymphocyte apoptosis and may involve Ras-MAPK dysregulation. Therefore, RASAL3 deficiency could serve as a common molecular denominator across these disorders.

To test this hypothesis, we developed an experimental system for the functional assessment of RASAL3 variants.

During the M2 internship, a reliable in vitro system was established for both T and B cell models, and a comprehensive experimental pipeline was set up to investigate the effects of the selected variants on RAS pathway activation following TCR or BCR stimulation.

Jurkat cells were shown to respond efficiently to anti-CD3 (OKT3) stimulation, exhibiting robust ERK phosphorylation, thereby validating their use as a suitable model for TCR-mediated Ras activation (Fig. 11). Similarly, B-lymphoblastoid cell lines (B-LCLs) demonstrated activation of the Ras-ERK signaling cascade upon BCR engagement (Fig.12).

Key molecular tools required for functional analysis were successfully validated. These included antibodies for the detection of RASAL3 (Fig.16), as well as key downstream effectors such as phosphorylated ERK (pERK), AKT (pAKT), and S6RP (pS6RP).

In addition, site-directed mutagenesis was performed to introduce the selected RASAL3 variants into the pCMV expression plasmid (Fig.19). The ERK pathway stimulation protocol was optimized in HEK293 cells, establishing them as a suitable intermediate system for the preliminary evaluation of the functional impact of each mutant (Fig.13-14). This setup will allow future transfection experiments to assess early signaling alterations before proceeding to the generation of viral vectors for transducing the previously validated Jurkat and B-LCL cellular models.

Nevertheless, several technical limitations were identified. CD3/CD28 beads did not induce robust ERK phosphorylation (Fig. 11), possibly due to short interaction times or suboptimal activation. This could be referred to the use of CD3/CD28-coated surfaces to enhance stimulation efficiency. Similarly, improved stimulation protocols for B-LCLs are required to align flow cytometry and Western blot data, potentially through longer stimulation or better antibody validation (Fig.12).

To address these challenges. Creating a *RASAL3* knockdown model via RNAi or CRISPR/Cas would enable a more comprehensive analysis of variant function (allowing the investigation of the functional impact of each variant in the context of partial or complete loss of function) and could serve as a negative control.

While the knockdown model could help assess the effects of reduced or absent RASAL3 activity, the co-expression system could better mimic the heterozygous state observed in patients. Together, these approaches could provide in future a more comprehensive understanding of the role of RASAL3 in T cell signaling and its contribution to immune dysregulation.

In addition to lymphoid models, in HEK cells, titrated transfection of *RASAL3* plasmid could reveal dose-response effects on Ras signaling. Optimization is also needed for simultaneous pERK and total ERK detection via Western blot; currently, this is hindered by antibodies raised in the same host

species. Solutions include using antibodies from different species or probing duplicate membranes.

Validating findings in patient-derived primary cells will be crucial to confirm and investigate links between molecular defects and clinical presentation. Moreover, extending functional assays to patient-derived primary cells will validate the results in more physiologically relevant context and it could provide evidence into the correlation between clinical manifestations and molecular defect. In addition to signaling pathway analyses, it could be important to investigate the impact of the variants on key cellular functions by performing assays such as proliferation assays (BrdU incorporation), apoptosis assays (Annexin V/PI staining), migration assays (3D migration assay) and cytokine production assays (intracellular cytokine staining). In particular, a recent paper shows that RASAL3 seems to interact with CCDC88 and ARGHEF2 in order to regulate leukocyte mobility and activation of immune e inflammatory response (Olivier et al., 2024).

Segregation analysis using family samples will help determine variant inheritance patterns and co-segregation with disease, strengthening pathogenicity evidence.

Further, exploring other downstream targets of TCR signal will allow to understand if other connected molecular pathways are affected by *RASAL3* variants. For example, RAS-GTP pull-down assay will quantify variations of active forms of RAS correlated with each variant. But also Rho-GTP investigation uncovers additional mechanisms by which RASAL3 influences immune cell function and homeostasis (Shin et al., 2018).

Furthermore, exploring the interaction between RASAL3 and CD229 is of great interest, as recent studies have shown that CD229 interacts with RASAL3 to activate the RAS/ERK pathway, promoting proliferation in multiple myeloma cells (Lin et al., 2022). Investigating this interaction in T cells could reveal novel regulatory pathways relevant to autoimmune disease pathogenesis.

It is also essential to consider compensatory mechanisms, such as expression of other RasGAPs. For instance, the expression of other RasGAP family members such as RASA1 could potentially compensate for the absence or dysfunction of RASAL3, thereby influencing the observed outcomes (Lubeck et al., 2015). Generating double knockdown models could help define its unique role. Notably, one patient in the study carries a potentially pathogenic *RASA1* variant, supporting the relevance of this axis.

Interestingly, although all variants were found in the same gene, they are associated with two distinct autoimmune conditions. A phenomenon that is not uncommon in the context of immune-related disorders. Indeed, it is well established that mutations in the same gene can lead to a spectrum of clinical manifestations, even among individuals carrying the identical variant, as observed in disorders such as ALPS-FAS, where partial clinical penetrance is frequent, or in cases involving Suppressor of cytokine signaling 1 (SOCS1) and Tyrosine-protein phosphatase non-receptor type 2 (PTPN2) mutations, which have been associated with diverse

phenotypes despite affecting the same locus (Jeanpierre et al., 2024; Hadjadj et al., 2020).

Pharmacological targeting of Ras/MAPK components (e.g., MEK or ERK inhibitors) could confirm pathway involvement and highlight therapeutic opportunities, especially if differential responses are observed in cells expressing WT versus mutant *RASAL3*.

Altogether, this work establishes the experimental framework for dissecting the impact of RASAL3 variants on immune cell signaling. Integrating genetic, biochemical, and functional data, opens the way for future studies aimed at elucidating the contribution of RASAL3 to the pathogenesis of pediatric autoimmunity and potentially uncovering new targets for precision medicine approaches.

BIBLIOGRAPHY

Aladjidi, N., Pincez, T., Rieux-Laucat, F., & Nugent, D. (2023). Paediatric-onset Evans syndrome: Breaking away from refractory immune thrombocytopenia. *British Journal of Haematology*, *203*(1), 28–35. https://doi.org/10.1111/bjh.19073

Audia, S., Grienay, N., Mounier, M., Michel, M., & Bonnotte, B. (2020). Evans' Syndrome: From Diagnosis to Treatment. *Journal of Clinical Medicine*, *9*(12), 3851. https://doi.org/10.3390/jcm9123851

Bonnerot, C., Briken, V., & Amigorena, S. (n.d.). *Intracellular signaling and endosomal trafficking of immunoreceptors Shared effectors underlying MHC class II-restricted antigen presentation*.

Chaplin, D. D. (2010). Overview of the immune response. *Journal of Allergy and Clinical Immunology*, *125*(2), S3–S23. https://doi.org/10.1016/j.jaci.2009.12.980

Courtney, A. H., Lo, W.-L., & Weiss, A. (2018). TCR Signaling: Mechanisms of Initiation and Propagation. *Trends in Biochemical Sciences*, *43*(2), 108–123. https://doi.org/10.1016/j.tibs.2017.11.008

Cyster, J. G., & Allen, C. D. C. (2019). B Cell Responses: Cell Interaction Dynamics and Decisions. *Cell*, *177*(3), 524–540. https://doi.org/10.1016/j.cell.2019.03.016

Degn, S. E., & Tolar, P. (2025). Towards a unifying model for B-cell receptor triggering. *Nature Reviews Immunology*, *25*(2), 77–91. https://doi.org/10.1038/s41577-024-01073-x

Downward, J. (2002). *TARGETING RAS SIGNALLING PATHWAYS IN CANCER THERAPY*.

Hadjadj, J., Aladjidi, N., Fernandes, H., Leverger, G., Magérus-Chatinet, A., Mazerolles, F., Stolzenberg, M.-C., Jacques, S., Picard, C., Rosain, J., Fourrage, C., Hanein, S., Zarhrate, M., Pasquet, M., Abou Chahla, W., Barlogis, V., Bertrand, Y., Pellier, I., Colomb Bottollier, E., … Rieux-Laucat, F. (2019). Pediatric Evans syndrome is associated with a high frequency of potentially damaging variants in immune genes. *Blood*, *134*(1), 9–21. https://doi.org/10.1182/blood-2018-11-887141

Hadjadj, J., Castro, C. N., Tusseau, M., Stolzenberg, M.-C., Mazerolles, F., Aladjidi, N., Armstrong, M., Ashrafian, H., Cutcutache, I., Ebetsberger-Dachs, G., Elliott, K. S., Durieu, I., Fabien, N., Fusaro, M., Heeg, M., Schmitt, Y., Bras, M., Knight, J. C., Lega, J.-C., … Rieux-Laucat, F. (2020). Early-onset autoimmunity associated with SOCS1 haploinsufficiency. *Nature Communications*, *11*(1), 5341. https://doi.org/10.1038/s41467-020-18925-4

Hahn, J. W., Yang, H. R., Moon, J. S., Chang, J. Y., Lee, K., Kim, G. A., Rahmati, M., Koyanagi, A., Smith, L., Kim, M. S., López Sánchez, G. F., Elena, D., Shin, J.-Y., Shin, J. I., Kwon, R., Kim, S., Kim, H. J., Lee, H., Ko, J. S., & Yon, D. K. (2023). Global incidence and prevalence of autoimmune hepatitis, 1970–2022: A systematic review and meta-analysis. *eClinicalMedicine*, *65*, 102280. https://doi.org/10.1016/j.eclinm.2023.102280

Jeanpierre, M., Cognard, J., Tusseau, M., Riller, Q., Bui, L.-C., Berthelet, J., Laurent, A., Crickx, E., Parlato, M., Stolzenberg, M.-C., Suarez, F., Leverger, G., Aladjidi, N., Collardeau-Frachon, S., Pietrement, C., Malphettes, M., Froissart, A., Bole-Feysot, C., Cagnard, N., … Mathieu,

A.-L. (2024). Haploinsufficiency in PTPN2 leads to early-onset systemic autoimmunity from Evans syndrome to lupus. *Journal of Experimental Medicine*, *221*(9), e20232337. https://doi.org/10.1084/jem.20232337

Kortum, R. L., Rouquette-Jazdanian, A. K., & Samelson, L. E. (2013). Ras and extracellular signal-regulated kinase signaling in thymocytes and T cells. *Trends in Immunology*, *34*(6), 259–268. https://doi.org/10.1016/j.it.2013.02.004

Lin, Z., Tang, X., Cao, Y., Yang, L., Jiang, M., Li, X., Min, J., Chen, B., Yang, Y., & Gu, C. (2022). CD229 interacts with RASAL3 to activate RAS/ERK pathway in multiple myeloma proliferation. *Aging*, *14*(22), 9264–9279. https://doi.org/10.18632/aging.204405

Liu, Y., Shepherd, E. G., & Nelin, L. D. (2007). MAPK phosphatases—Regulating the immune response. *Nature Reviews Immunology*, *7*(3), 202–212. https://doi.org/10.1038/nri2035

Lubeck, B. A., Lapinski, P. E., Oliver, J. A., Ksionda, O., Parada, L. F., Zhu, Y., Maillard, I., Chiang, M., Roose, J., & King, P. D. (2015). Cutting Edge: Codeletion of the Ras GTPase-Activating Proteins (RasGAPs) Neurofibromin 1 and p120 RasGAP in T Cells Results in the Development of T Cell Acute Lymphoblastic Leukemia. *The Journal of Immunology*, *195*(1), 31–35. https://doi.org/10.4049/jimmunol.1402639

Lucas, C. L., & Lenardo, M. J. (2015). Identifying genetic determinants of autoimmunity and immune dysregulation. *Current Opinion in Immunology*, *37*, 28–33. https://doi.org/10.1016/j.coi.2015.09.001

Lv, T., Li, M., Zeng, N., Zhang, J., Li, S., Chen, S., Zhang, C., Shan, S., Duan, W., Wang, Q., Wu, S., You, H., Ou, X., Ma, H., Zhang, D., Kong, Y., & Jia, J.

(2019). Systematic review and meta-analysis on the incidence and prevalence of autoimmune hepatitis in Asian, European, and American population. *Journal of Gastroenterology and Hepatology*, *34*(10), 1676–1684. https://doi.org/10.1111/jgh.14746

Muro, R., Nitta, T., Kitajima, M., Okada, T., & Suzuki, H. (2018). Rasal3-mediated T cell survival is essential for inflammatory responses. *Biochemical and Biophysical Research Communications*, *496*(1), 25–30. https://doi.org/10.1016/j.bbrc.2017.12.159

Muro, R., Nitta, T., Okada, T., Ideta, H., Tsubata, T., & Suzuki, H. (2015). The Ras GTPase-Activating Protein Rasal3 Supports Survival of Naive T Cells. *PLOS ONE*, *10*(3), e0119898. https://doi.org/10.1371/journal.pone.0119898

Nastasio, S., Sciveres, M., Francalanci, P., & Maggiore, G. (2024). Pediatric Autoimmune Hepatitis. *Pediatric Reports*, *16*(1), 110–113. https://doi.org/10.3390/pediatric16010011

Olivier, J.-F., Langlais, D., Jeyakumar, T., Polyak, M. J., Galarneau, L., Cayrol, R., Jiang, H., Molloy, K. R., Xu, G., Suzuki, H., LaCava, J., Gros, P., & Fodil, N. (2024). CCDC88B interacts with RASAL3 and ARHGEF2 and regulates dendritic cell function in neuroinflammation and colitis. *Communications Biology*, *7*(1), 77. https://doi.org/10.1038/s42003-023-05751-9

Powell, J. D., Pollizzi, K. N., Heikamp, E. B., & Horton, M. R. (2012). Regulation of Immune Responses by mTOR. *Annual Review of Immunology*, *30*(1), 39–68. https://doi.org/10.1146/annurev-immunol-020711-075024

Saito, S., Kawamura, T., Higuchi, M., Kobayashi, T., Yoshita-Takahashi, M., Yamazaki, M., Abe, M., Sakimura, K., Kanda, Y., Kawamura, H., Jiang, S., Naito, M., Yoshizaki, T., Takahashi, M., & Fujii, M. (2015). RASAL3, a novel hematopoietic RasGAP protein, regulates the number and functions of NKT cells. *European Journal of Immunology*, *45*(5), 1512–1523. https://doi.org/10.1002/eji.201444977

Scheffzek, K., & Shivalingaiah, G. (n.d.). *Ras-Specific GTPase-Activating Proteins—Structures, Mechanisms, and Interactions*.

Shah, K., Al-Haidari, A., Sun, J., & Kazi, J. U. (2021). T cell receptor (TCR) signaling in health and disease. *Signal Transduction and Targeted Therapy*, *6*(1), 412. https://doi.org/10.1038/s41392-021-00823-w

Shin, Y., Kim, Y., Kim, H., Shin, N., Kim, T., Kwon, T., Choi, J., & Chang, J.-S. (2018). RASAL3 preferentially stimulates GTP hydrolysis of the Rho family small GTPase Rac2. *Biomedical Reports*. https://doi.org/10.3892/br.2018.1119

Terziroli Beretta-Piccoli, B., Mieli-Vergani, G., & Vergani, D. (2022). Autoimmmune hepatitis. *Cellular & Molecular Immunology*, *19*(2), 158–176. https://doi.org/10.1038/s41423-021-00768-8

Wen, Y., Jing, Y., Yang, L., Kang, D., Jiang, P., Li, N., Cheng, J., Li, J., Li, X., Peng, Z., Sun, X., Miller, H., Sui, Z., Gong, Q., Ren, B., Yin, W., & Liu, C. (2019). The regulators of BCR signaling during B cell activation. *Blood Science*, *1*(2), 119–129. https://doi.org/10.1097/BS9.0000000000000026

Yasmeen, F. (2024). *Understanding Autoimmunity: Mechanisms, Predisposing Factors, and Cytokine Therapies*.

Appendix

Preliminary protocols and optimization attempts

To develop the optimal protocol for OKT3-mediated stimulation, it was initially tested stimulation with recombinant human IL-2 (Sigma-Aldrich, Cat# I0779). Interleukin-2 (IL-2) is a key cytokine secreted by activated T cells that promotes antigen-driven clonal expansion by activating the PI3K/STAT and MAPK pathways.

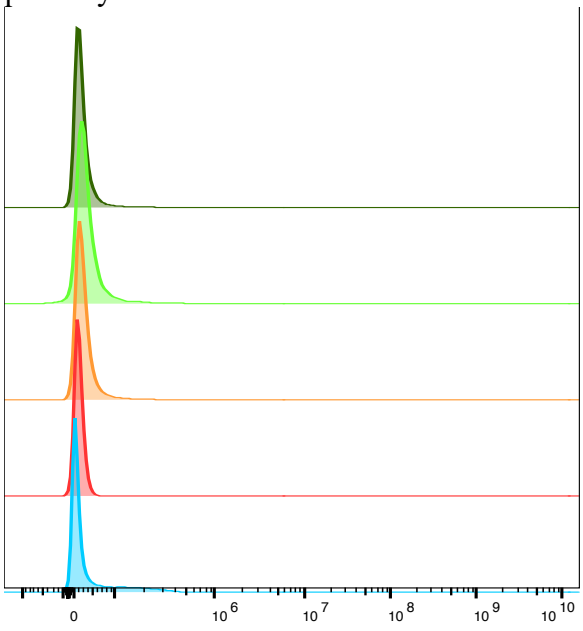

	Sample Name	Subset Name	Count
	A5_pERK IL2 1000U_ml.fcs	Single Cells	23209
	A4_pERK IL2 100U_ml.fcs	Single Cells	19372
	A3_pERK IL2 10U_ml.fcs	Single Cells	21087
	A2_Iso.fcs	Single Cells	15946
	A1_NS.fcs	Single Cells	21749

Figure 21: Flow cytometry analysis of Jurkat cells stimulated with varying concentrations of IL-2.

IL-2 stimulation failed to induce significant phosphorylation of ERK (pERK) in Jurkat cells. A possible explanation for this result is that Jurkat cells, due to their immortalized nature, may express low or undetectable levels of the IL-2 receptor alpha chain (CD25), which is essential for high-affinity IL-2 signaling.

Following these results, it was explored pERK induction using OKT3-mediated stimulation. Prior to defining the final protocol, experimental parameters were optimized based on a plate-bound OKT3 stimulation strategy. The desired concentration of OKT3 antibody was diluted in PBS and coated onto a 96-well plate overnight at 4 °C. The next day, Jurkat cells were added to the wells, and stimulation was carried out by incubating the plate at 37 °C for 15 minutes. After stimulation, cells were transferred from the coated wells into other wells for downstream analysis. The levels of pERK detected with this protocol were suboptimal. To enhance the response, a crosslinker-based stimulation protocol has been suggested.

The influence of Jurkat cell culture conditions on pERK levels was investigated. In particular, the effect of medium replacement was analyzed to assess whether it alters pERK levels as a result of cellular responses related to proliferation or stress.

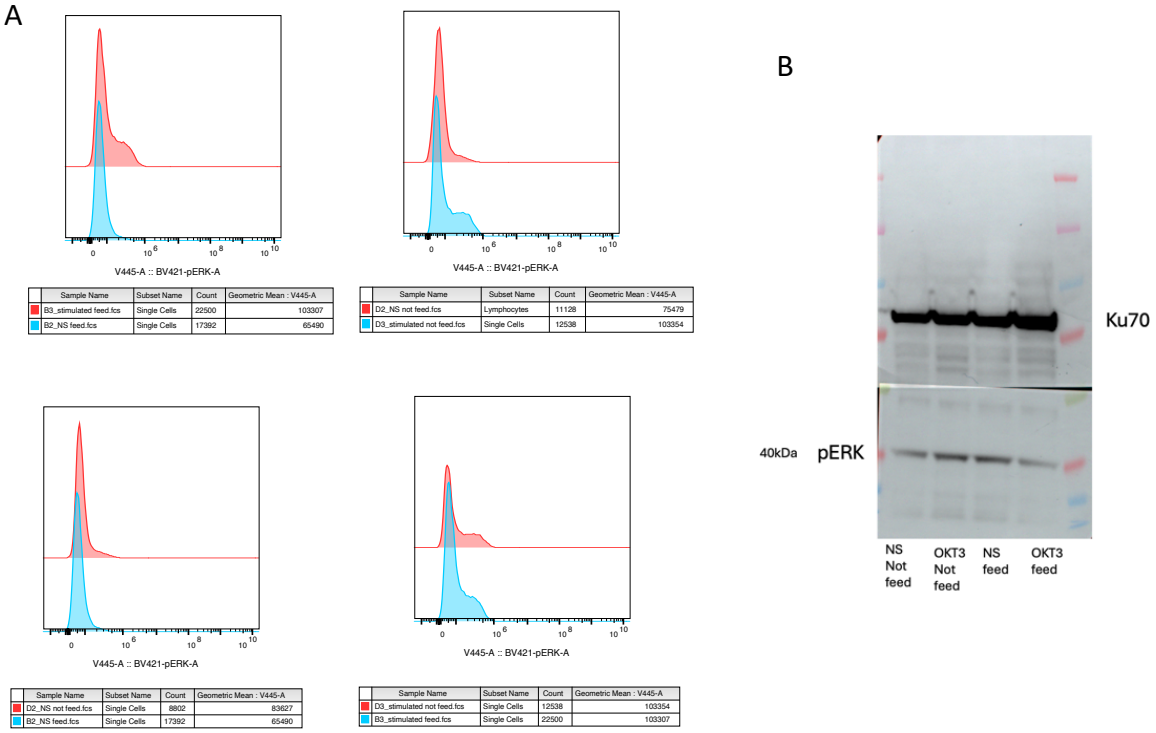

Figure 22: Analysis of pERK after OKT3 stimulation with different culture conditions. Feed condition for detection in cells that have faced the changing of medium the day of the analysis; not feed condition corresponds to the culture of cells with medium changed the day before. (A) flow cytometry analysis of level of pERK detected in each condition. (B) western blot analysis.

Performing the assay immediately after changing the culture medium significantly affected the levels of phosphorylated ERK (pERK) detected. Based on flow cytometry data (fig. 22), medium replacement alone resulted in a marked increase in pERK levels, with geometric mean fluorescence intensity rising by approximately 50–60% compared to non-fed conditions. This suggests that medium renewal triggers a signaling response potentially linked to nutrient sensing or cellular stress recovery mechanisms.

Therefore, it is crucial to maintain consistent culture conditions when performing the assay. Specifically, avoiding medium change on the same day of the assay is recommended to minimize background activation of the ERK pathway.

Although a clear pERK signal was detected by Western blot across all tested conditions, no significant differences in band intensity were observed (fig.22B). This could be due to suboptimal stimulation in the experimental setup, possibly related to the use of plate-bound OKT3 antibody, which may not have effectively triggered robust ERK activation.

Optimization of RASAL3 Western Blot: Antibody Selection

Initially analysis was performed by using RASAL3 antibody produced by Invitrogen already present in the lab, Anti-RASAL3 Polyclonal Antibody (Cat# PA5-24097). But it was established that the antibody was not specific for detecting the protein of interest in the cellular models chosen for the project.

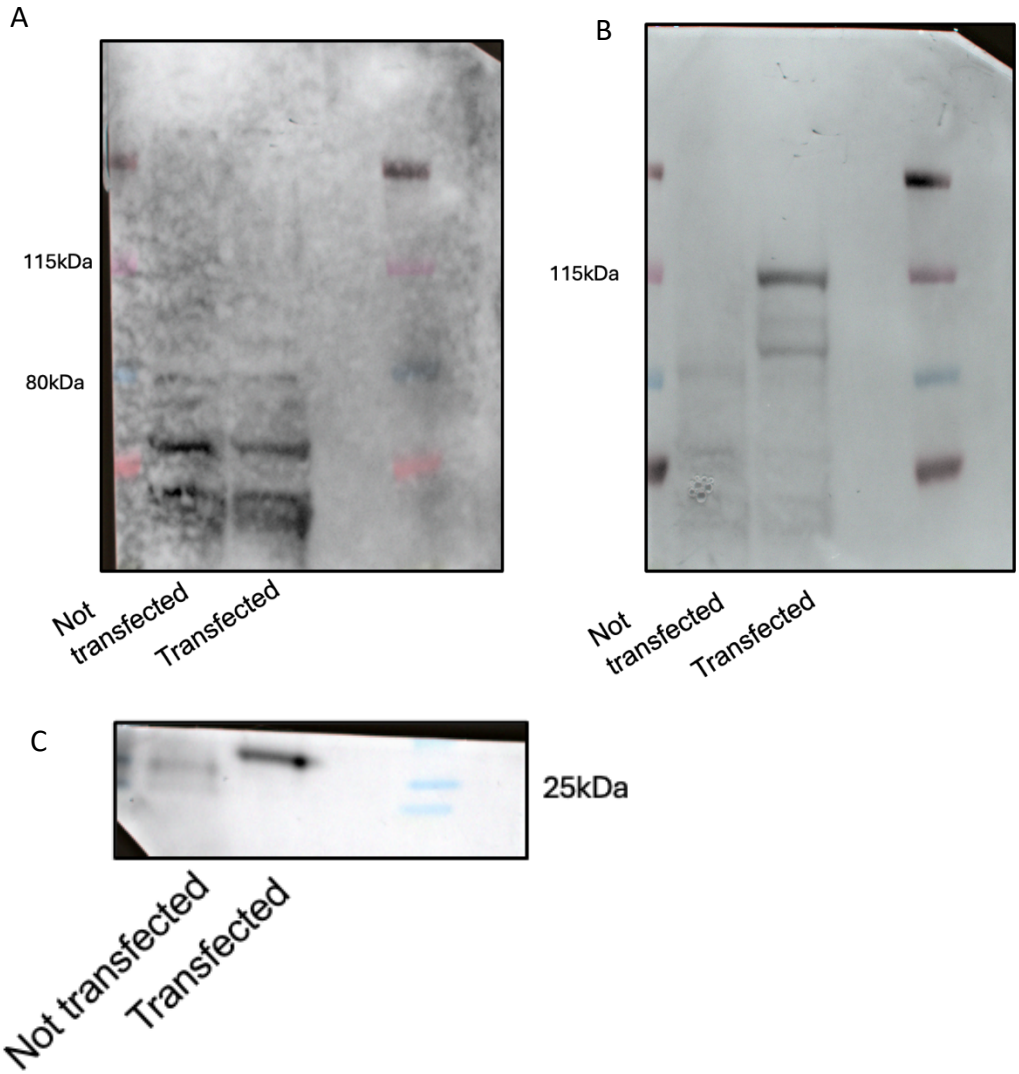

Figure 23: Western blot comparing transfected and non-transfected HEK293 cells.
(A) Detection of RASAL3 protein using the anti-RASAL3 antibody (Invitrogen, Cat# PA5-24097).
(B) Detection of the HA-tag using anti-HA antibody, confirming expression of the pCMV-HA-RASAL3 WT plasmid in transfected cells.
(C) Detection of GFP using anti GFP antibody, confirming efficient transfection Non-transfected cells served as a negative control in all blots.

The antibody used for detecting RASAL3 did not show the expected band in transfected HEK cells (Fig.23A), despite the successful detection of the HA-tagged RASAL3 by the anti-HA antibody (Fig.23B). Based on these results, we decided to select and use an alternative, more specific antibody against RASAL3 for subsequent experiments (Proteintech, Cat. #21164-1-AP) (Fig. 16).

First transfection HEK cells with pCMV-HA-RASAL3 mutants and WT

Once obtained and validated the pCMV plasmids carrying the mutations of interest HEK cells have been transfected to test the variation of phosphorylated targets.

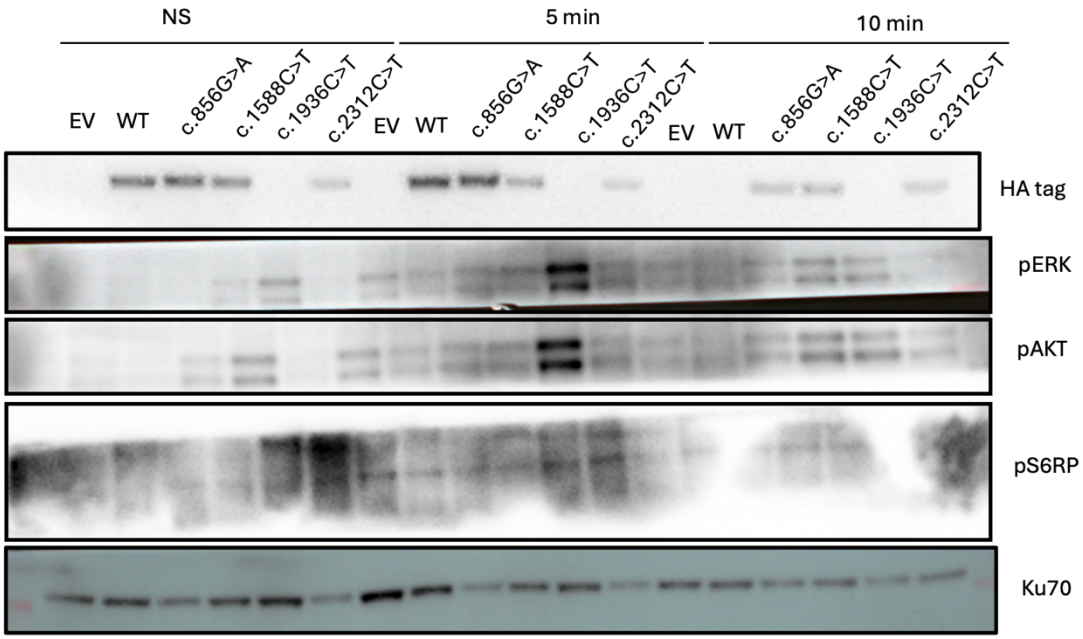

Figure 24: HEK cell transfection with pCMV plasmids encoding either wild-type (WT) or mutant forms of the RASAL3 sequence. EV: empty vector (plasmid without insert); WT: plasmid carrying the wild-type RASAL3 sequence; NS is non stimulated; 5min or 10 min are the stimulation conditions based on adding FBS. Protein expression was assessed by immunodetection of HA tag, phosphorylated S6 ribosomal protein (pS6RP), phosphorylated ERK (pERK), and phosphorylated AKT (pAKT).

The detection of the HA tag confirmed specific expression of the transfected constructs and excluded the presence of non-specific bands observed in previous experiments. These earlier unspecific signals likely resulted from antibody cross-reactivity rather than true *RASAL3*-derived products (Fig. 17-23). Notably, the mutant plasmid carrying the c.1936C>T variant did not yield an HA-tagged band, potentially due to technical issues during transfection or protein expression. The detection of phosphorylated downstream targets (pS6RP, pERK, pAKT) was suboptimal, limiting the interpretation of signaling differences among experimental conditions. Variability in housekeeping protein levels suggests differences in the amount of protein loaded across samples.